Received January 13, 2020, accepted February 19, 2020, date of publication February 27, 2020, date of current version March 10, 2020.

Digital Object Identifier 10.1109/ACCESS.2020.2976595

A Bayesian Optimization AdaBN-DCNN Method With Self-Optimized Structure and Hyperparameters for Domain Adaptation Remaining Useful Life Prediction

JIALIN LI[1] **AND DAVID HE**[2]
[1]School of Mechanical Engineering and Automation, Northeastern University, Shenyang 110819, China
[2]Department of Mechanical and Industrial Engineering, The University of Illinois at Chicago, Chicago, IL 60607, USA

Corresponding author: David He (davidhe@uic.edu)

ABSTRACT The prediction of remaining useful life (RUL) of mechanical equipment provides a timely understanding of the equipment degradation and is critical for predictive maintenance of the equipment. In recent years, the applications of deep learning (DL) methods to predict equipment RUL have attracted much attention. There are two major challenges when applying the DL methods for RUL prediction: (1) It is difficult to select the prediction model structure and hyperparameters such as network depth, learning rate, batch size, and etc. (2) The developed prediction model is domain dependent, i.e., it can only give good prediction performance in one data domain (one particular type of working conditions and fault modes). In order to meet the challenges, a novel RUL prediction method developed using a deep convolutional neural network (DCNN) combined with Bayesian optimization and adaptive batch normalization (AdaBN) is presented in this paper. The proposed RUL prediction model is validated by the turbofan engine degradation simulation dataset provided by NASA. The prediction results show that the proposed prediction model provides better prediction results than model structures obtained by random search and grid search. The results also show that the domain adaptation capability of the prediction model has been improved.

INDEX TERMS Remaining useful life prediction, Bayesian optimization, adaptive batch normalization, domain adaptation.

I. INTRODUCTION

In recent years, mechanical equipment has become more and more complicated with the development of new sciences and technologies. Therefore, the prognostics and health management (PHM) of mechanical equipment is becoming a more attractive topic. PHM provides a comprehensive management solution such as remaining useful life (RUL) prediction for maintaining the health of mechanical systems [1]. Over recent years, the research on developing data-driven RUL prediction methods has attracted much attention [2], [3]. Deep learning (DL) methods as a type of data-driven methods can achieve nonlinear mapping between training data and targets. Papers on developing DL based RUL prediction approaches have reported its superiority over other traditional data-driven approaches such as statistical approaches and so on [4], [5].

The associate editor coordinating the review of this manuscript and approving it for publication was Zhaojun Li.

However, there are some challenges when using DL for RUL prediction such as network structure selection, hyperparameter optimization, and domain dependent etc. The purpose of the proposed method is to address these challenges.

Ren *et al.* [6] proposed a novel feature extraction method spectrum-principal-energy-vector to obtain the eigenvector. A deep convolution neural network was used to predict bearing RUL. Yu *et al.* [7] proposed an autoencoder based on a bidirectional RNN to convert multi-sensor data into low-dimensional data in an unsupervised way. It was then used to construct a one-dimensional HI to reflect the degradation process of the device. Because learning features from a fixed window size may result in changes in local features and therefore may affect the prediction results, Zhao *et al.* [8] proposed a RUL prediction method based on the trend feature of the total time series representing degradation. An empirical mode decomposition (EMD) method was used to decompose and reconstruct the signals to obtain trend features. And then, the conditional neural processes were used to evaluate the trend features. Finally, the RUL was predicted using the best trend features as an input to the RNN. In order to extract as much information as possible from the observed sequence, Elsheikh *et al.* [9] proposed a bidirectional hand-shaking long short-term memory (LSTM) to predict the RUL of a turbofan engine. Wu *et al.* [10] applied vanilla LSTM for RUL estimation of engineering systems, and proposed a dynamic differential technique to extract inter-frame information to enhance the cognitive ability of the degradation process model. Rigamonti *et al.* [11] used echo state networks (ESNs) to predict the RUL of industrial components such as turbofan engine. The innovation of the proposed method is to use a separate ESN memory capacity to aggregate ESNs results in a dynamic process and an additional ESN to estimate RUL by the mean variance estimation (MVE) method. Yang *et al.* [12] proposed an Elman neural network (ENN) based method to predict the RUL of an ultrasonic motor. The principal component analysis (PCA) was used to extract the motor degradation index from the monitoring data. An improved particle swarm optimization algorithm (IPSO) was used to improve the prediction accuracy of the ENN. Li *et al.* [13] used short-time Fourier transform (STFT) to extract time-frequency domain information from the rolling bearing dataset. A convolutional neural network (CNN) was used to achieve multi-scale feature fusion and intelligent RUL prediction. Zhu *et al.* [14] applied wavelet transform (WT) to obtain useful information, and then used a bilinear interpolation method to reduce the features. A multiscale convolutional neural network (MSCNN) model structure was proposed to save global and local information simultaneously to predict the RUL.

Among the DL based methods for mechanical equipment RUL prediction mentioned above, two important aspects related to model development need to be addressed: (1) selection of the model structure and hyperparameters (e.g. learning rate, batchsize, momentum etc.), and (2) domain adaptability of the developed model. The network structure and hyperparameter selection methods include: manual search, grid search, random search, and advanced optimization methods [15]. Most of the existing approaches develop and train the prediction model using manual search strategy [16], [17]. The model structure and training hyperparameters were chosen manually based on an understanding of the prediction methods and the experience of previous researchers. The grid search method is to equidistantly select several parameter values within the range to develop the models separately. Then the model with the best predicted result is selected as the target model. The references [8]–[10] applied the grid search method to select the optimal structure of the model. The random search method is to randomly select several sets of parameters within the range for model development. It has been empirically and theoretically proven that the random search is more effective for the hyperparameter optimization than for the grid search [18]. The domain adaptability of the prediction model is also an important performance quality indicator for model evaluation. In order to improve the domain adaptability of the developed prediction model, many attempts have been made by the researchers. Transfer learning (TL) [19], [20] strategy has proven to be effective for improving the adaptability of the model in many cases. A sufficient number of degraded samples for data-driven prediction are difficult to obtained, Zhang *et al.* [21] proposed a bi-directional long short-term memory (BLSTM) based TL method to predict RUL. The prediction model trained on one dataset can be used to predict the relevant target dataset by fine-tuning the TL strategy. In addition, adaptive batch normalization (AdaBN) [22], [23] algorithm can also be used to improve the domain adaptability of the prediction model. Initially, batch normalization (BN) was used to help stochastic gradient descent (SGD) optimization by adjusting the distribution of each layer of the output in the network [24]. It was later found that domain adaptation can be achieved by retraining the offset parameters in the BN unit.

To address the two issues encountered in developing DL based prediction methods mentioned above, this paper proposes a RUL prediction method based on deep convolutional neural network (DCNN) combined with Bayesian optimization [25] and AdaBN algorithm. The Bayesian optimization method is used to automatically select the network structure and hyperparameters. The AdaBN algorithm is used to improve the ability of predictive models to adapt to different data domains (DDs). The main contributions of this paper are summarized as follows:

(1) This paper provides an optimization strategy for prediction network structure and hyperparameters based on data-driven method. The Bayesian optimization method is used to realize the self-selection of the network structure and hyperparameters. Compared with manual search and grid search, the proposed method can develop a RUL prediction model with better performance in a shorter time.

(2) In this paper, the BN unit is added in the DCNN, and the prediction tasks of different DDs are adapted by modifying the offset parameters of the BN unit. Compared with the commonly used domain adaptation algorithm-TL, the AdaBN method requires fewer parameters to be fine-tuned in different DDs, which means that the calculation effort is reduced and the adaptation time is shortened.

The rest of the paper is organized as follows. In Section II, related background knowledge is provided. The proposed method is explained in Section III. In Section IV, the C-MAPSS dataset and validation results are described. Finally, Section V concludes the paper.

II. BACKGROUNDS

A. BAYESIAN OPTIMIZATION

The data-driven deep learning methods are more attractive because they are not affected by the physical structure of the system and can be developed rapidly. However, the hyperparameters of the deep learning network such as

TABLE 1. Procedure of the Bayesian optimization for deep learning hyperparameters.

```
Algorithm 1: Bayesian Optimization
Input: Within the range, randomly select $i$ sets of hyperparameters
       $\chi_i$. Each set contains $m$ hyperparameters $hp_{1:m} \epsilon \chi$, black-box
       function $f$, and the number of optimization iterations $n$.

Step 1. Global exploration:
        ● Calculate observations $f_{1:i} = f(x_{1:i})$, i.e., $D_{1:n} = [x_{1:i}, f(x_{1:i})]$.
        ● Predict black-box function $f'_{1:i} \sim N(m(x_{1:n}), \boldsymbol{K})$, where $\boldsymbol{K}$ is
          shown in Equation (6).

Step 2. Determine the next observation point $x_{i+1}$:
        ● According to the principle of GP distribution, $f(x_{1:i})$ and
          $f(x_{i+1})$ obey the joint Gaussian distribution as:
          $\begin{bmatrix} f(x_{1:i}) \\ f(x_{i+1}) \end{bmatrix} \sim N\left(m\left(\begin{bmatrix} x_{1:i} \\ x_{i+1} \end{bmatrix}\right), \begin{bmatrix} \boldsymbol{K} & k_* \\ k_*^T & k(x_{i+1}, x_{i+1}) \end{bmatrix}\right)$.
        ● The probability distribution of $f(x_{i+1})$ can be easily obtained
          as: $P((f(x_{i+1}|D_{1:i}, x_{i+1})) \sim N(\mu(x_{i+1}), \sigma^2(x_{i+1}))$, where
          $\mu(x_{i+1}) = k_*^T \boldsymbol{K}^{-1} f(x_{1:i})$ ; $\sigma^2(x_{i+1}) = k(x_{i+1}, x_{i+1}) - k_*^T \boldsymbol{K}^{-1} k_*$.
        ● $x_{i+1}$ is determined by acquisition function $Acq(x)$, i.e., $x_{i+1} =$
          $argmax_{x_{i+1} \epsilon \chi} Acq(x_{i+1})$. A lower confidence bound
          acquisition functions can be used: $Acq_{LCB}(x_{i+1}) =$
          $k\sigma(x_{i+1}) - \mu(x_{i+1})$.
        ● The next observation point can be calculated as $x_{i+1} =$
          $argmax_{x \epsilon \chi}[k\sigma(x_{i+1}) - \mu(x_{i+1})]$.

Step 3. Calculate $f(x_{i+1})$ and update prediction function $f'_{1:i+1}$:
        ● Use $x_{i+1}$ determined in Step 2 to compute the new
          observations $f_{i+1} = f(x_{i+1})$.
        ● Predict black-box function $f'_{1:i+1} \sim N(m(x_{1:i+1}), \boldsymbol{K})$.

Step 4. For $n = 1, 2, \ldots$ do
        ● Repeat Step 2 and Step 3
        End

Output: Predicted black-box function $f'_{1:i+n}$; the smallest observation $f^+$
        and the corresponds hyperparameter set $x_{\text{best}}$.
```

the learning rate, batchsize, and the number of network layers, have a great influence on the network capability. This paper uses Bayesian optimization [26] to search for the best hyperparameters. First of all, one needs to select the hyperparameters to be optimized $\{hp_{1:m} \epsilon \chi\}$. It is assumed that the hyperparameters and the deep learning error (DLE) can be expressed by the black-box function f, i.e., DLE $= f(\chi)$. As shown in Equation (1), the purpose of Bayesian optimization is to find the point x_{best} with the minimal DLE value.

$$x_{best} = argmin_{x \epsilon \chi} f(x) \tag{1}$$

The steps of Bayesian optimization procedure for deep learning hyperparameters are shown in Table 1.

The Bayesian optimization mainly repeats the two steps of Gaussian process regression and acquisition function. Bayesian optimization includes two processes of "exploitation" and "exploration". The posterior distribution of the objective function is updated by successively adding observation sample points until the posterior distribution substantially conforms to the true distribution. The acquisition function can consider both "exploitation" and "exploration" to determine the next observation point x_{best}. In Step 1, the selection of the initial observation points $x_{1:i}$

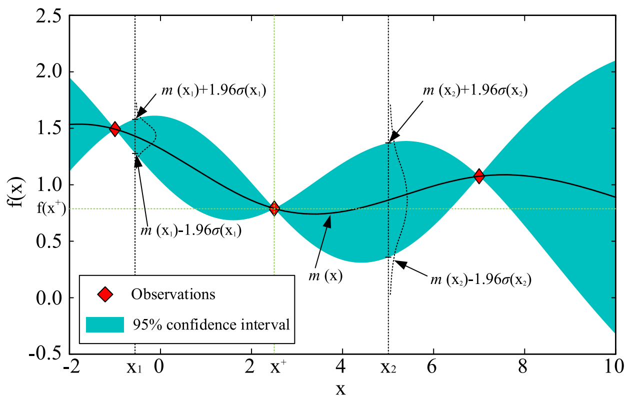

FIGURE 1. Example of 1-D Gaussian process with 3 observations.

within the range of values is global exploration. In Step 2, the distribution probability of $f(x_{i+1})$ is calculated according to the observation points $f(x_{1:i})$ and the rule of joint Gaussian distribution. Then, the position of the next observation point can be obtained in combination with the acquisition function. In Step 3, calculate $f(x_{i+1})$ and update the prediction function $f'_{1:i+1}$. Finally, repeat Steps 2 and 3. The hyperparameter set corresponding to the minimum value in all observation points is the best set.

Next, Gaussian process priors with Gaussian noise are introduced in Section II-A-1), kernel function options in Section II-A-2), and acquisition functions options in Section II-A-3).

1) GAUSSIAN PROCESS PRIORS

The Gaussian process (GP) [27] is a set of random variables so that any finite numbers of random variables have a joint Gaussian distribution. The GP can be represented entirely by the mean function and covariance function. The mean function $m(x)$ and covariance function $k(x, x')$ are expressed in Equations (2) and (3) as:

$$m(x) = E[f(x)] \tag{2}$$

$$k(x, x') = E[(f(x) - m(x))(f(x') - m(x'))] \tag{3}$$

Therefore $f(\mathrm{x})$ obeys the GP can be expressed as:

$$f(x) \sim GP[m(x), k(x, x')] \tag{4}$$

Fig. 1 shows a simple one-dimensional (1-D) GP with 3 observations.

The function $f(x)$ is a GP, and the three observation points are x_o^1, x_o^2, and x_o^3, respectively. So the joint distribution of the variables $f(x_o^1)$, $f(x_o^2)$, and $f(x_o^3)$ is a Gaussian distribution. The solid black line in Fig. 1 is the mean of the function $f(x)$ predicted by the GP through the observation point. The shaded area represents the 95% confidence interval for the Gaussian distribution of the function $f(x)$. It ranges from $m(x) - 1.96\sigma(x)$ to $m(x) + 1.96\sigma(x)$, which $m(x)$ and $\sigma(x)$ are prediction GP mean and standard deviation. x_1 and x_2 are two randomly selected points in the range of x, and the dotted line is a normal distribution of the $f(x)$ value. x^+ is the point at which the $f(x)$ value is the minimum for all observation points.

A commonly used squared exponential covariance function is shown in Equation (5). More other covariance functions are described in details in Section II-A-2). It can be known from Equation (5) that when the two points x_1 and x_2 are close, the $k(x_i, x_j)$ value approaches 1, i.e., the mutual influence of the two points is larger. On the contrary, when the two points are far away, the $k(x_i, x_j)$ value approaches 0, i.e., the interaction between the two points is weak.

$$k\left(x_i, x_j\right) = exp[-\frac{1}{2}\left(x_i - x_j\right)^2] \tag{5}$$

When Gaussian priors are performed on n observation points, it is known $D_{1:n} = \{x_{1:n}, f(x_{1:n})\}$, and the function values $f(x_{1:n})$ are obey to a multivariate normal distribution, i.e., $f(x_{1:n}) \sim N(m(x_{1:n}), \boldsymbol{K})$. And the kernel matrix of multivariate normal distribution is expressed as:

$$\boldsymbol{K} = \begin{bmatrix} k(x_1, x_1) & \cdots & k(x_1, x_n) \\ \vdots & \ddots & \vdots \\ k(x_n, x_1) & \cdots & k(x_n, x_n) \end{bmatrix} \tag{6}$$

The optimization is achieved by continuously increasing the observation points and performing repeating the Gaussian process prior until the prediction model is close to the real function $f(x)$. Therefore, the choice of the location of the observation point x is crucial. It is known that there has n observation points $D_{1:n} = \{x_{1:n}, f(x_{1:n})\}$. Then one needs to consider the next observation point x_{n+1} and the corresponding function value $f(x_{n+1})$. According to the principle of GP distribution, $f(x_{1:n})$ and $f(x_{n+1})$ obey the joint Gaussian distribution as:

$$\begin{bmatrix} f(x_{1:n}) \\ f(x_{n+1}) \end{bmatrix} \sim N\left(m\left(\begin{bmatrix} x_{1:n} \\ x_{n+1} \end{bmatrix}\right), \begin{bmatrix} \boldsymbol{K} & k_* \\ k_*^T & k(x_{n+1}, x_{n+1}) \end{bmatrix}\right) \tag{7}$$

where k$_*$ can expressed as:

$$k_* = [k\left(x_{n+1}, x_1\right), k\left(x_{n+1}, x_2\right) \cdots k(x_{n+1}, x_n)] \tag{8}$$

According to the mention above, the probability distribution of $f(x_{n+1})$ can be easily obtained as:

$$P((f(x_{n+1} \mid D_{1:n}, x_{n+1})) \sim N(\mu(x_{n+1}), \sigma^2(x_{n+1})) \tag{9}$$

where $\mu\left(x_{n+1}\right)$ and $\sigma^2\left(x_{n+1}\right)$ can be expressed as:

$$\mu\left(x_{n+1}\right) = = k_*^T \boldsymbol{K}^{-1} f(x_{1:n}) \tag{10}$$

$$\sigma^2\left(x_{n+1}\right) = k\left(x_{n+1}, x_{n+1}\right) - k_*^T \boldsymbol{K}^{-1} k_* \tag{11}$$

The derivation of the above equations is based on a noise-free environment. However, a noise-free environment in practical applications is rare. For example, applying a Gaussian process to fit the relationship between DLE and hyperparameters. Setting the same hyperparameters for multiple trials may result in different results. This shows that it is a noisy data environment. As shown in Equation (12), y is the signal after noise addition, where noise $\varepsilon \sim N(0, \sigma_{\text{noise}}^2)$. And the kernel matrix of multivariate normal distribution in Equation (6) is changes as shown in Equation (13).

$$y = f\left(x\right) + \varepsilon \tag{12}$$

$$\boldsymbol{K} = \begin{bmatrix} k(x_1, x_1) & \cdots & k(x_1, x_n) \\ \vdots & \ddots & \vdots \\ k(x_n, x_1) & \cdots & k(x_n, x_n) \end{bmatrix} + \sigma_{noise}^2 I \tag{13}$$

Similarly, the probability distribution of $f(x_{n+1})$ in a noisy environment is also changed, and can be expressed as Equations (14-16) as:

$$P((f(x_{n+1} \mid D_{1:n}, x_{n+1})) \sim N(\mu\left(x_{n+1}\right), \sigma^2\left(x_{n+1}\right) + \sigma_{noise}^2) \tag{14}$$

$$\mu\left(x_{n+1}\right) = k_*^T [\boldsymbol{K} + \sigma_{noise}^2 I]^{-1} f(x_{1:n}) \tag{15}$$

$$\sigma^2\left(x_{n+1}\right) = k\left(x_{n+1}, x_{n+1}\right) - k_*^T [\boldsymbol{K} + \sigma_{noise}^2 I]^{-1} k_* \tag{16}$$

2) KERNEL FUNCTION OPTIONS

The kernel function [28] has a crucial influence on the GP, which can affect the smoothness of the fitted curve. Equation (5) shows the standard squared exponential kernel. It can be seen from the equation that the points x_i and x_j with the same distance have the same covariance for different data environments. Therefore, when faced with a variety of complex prediction tasks, the standard squared exponential kernel is actually a little naive. An effective improvement method is to add hyperparameters in the kernel function to play a better role in a variety of data environments. The vector θ can be applied to parameterize the kernel function, which can be expressed as $k\left(x_i, x_j | \theta\right)$. In general, the parameterization of the kernel function is adjusted by parameters the signal standard deviation σ_f and the characteristic length scale σ_l. The characteristic length scale briefly defines the distance that the input value becomes irrelevant to the response value. By defining $\theta_1 = log\sigma_l$ and $\theta_2 = log\sigma_f$, the parameters σ_l and σ_f can be enforced greater than 0.

The improved squared exponential kernel: the results of parameterizing the kernel function in Equation (5) are as follows:

$$k\left(x_i, x_j | \theta\right) = \sigma_f^2 exp(-\frac{(x_i - x_j)^2}{\sigma_l^2}) \tag{17}$$

where σ_l is the characteristic length scale, and σ_f is the signal standard deviation.

In addition, other kernel functions commonly used for Bayesian optimization are the Matern class. The kernel Matern 3/2 and Matern 5/2 are defined as:

$$k\left(x_i, x_j | \theta\right) = \sigma_f^2 (1 + \frac{\sqrt{3}\, r}{\sigma_l}) exp(-\frac{\sqrt{3} r}{\sigma_l}) \tag{18}$$

$$k\left(x_i, x_j | \theta\right) = \sigma_f^2 (1 + \frac{\sqrt{5}\, r}{\sigma_l} + \frac{5r^2}{3\sigma_l^2}) exp(-\frac{\sqrt{5}\, r}{\sigma_l}) \tag{19}$$

where $r = \sqrt{(x_i - x_j)}^2$.

3) ACQUISITION FUNCTIONS OPTIONS

The Bayesian optimization process is accomplished by continuously adding observation points and performing Gaussian process priors. Therefore, the choice of observation points will directly affect the performance of the GP, further affecting the distribution of predicted function f. A "goodness" observation point can shorten the number of Gaussian process iterations, so that the Gaussian posterior distribution is closer to the actual function f. Based on the observation points $D_{1:n} = \{x_{1:n}, f(x_{1:n})\}$ and the posterior distribution function Q, the acquisition function is applied to find the next observation point x_{next}.

As shown in Equation (20), the next observation point x_{next} at which the acquisition function $Acq(x)$ has the maximum value, i.e., the point having the best potential to make the x_{best}.

$$x_{next} = argmax_{x\epsilon\chi} Acq(x) \tag{20}$$

There are many types of acquisition functions [29], and the three commonly used include confidence bound criteria, probability of improvement (PI), and expected improvement (EI).

The confidence bound criteria contains: lower confidence bound (LCB) and upper confidence bound (UCB). The LCB is used to find the minimum value of the function, and the UCB is used to find the maximum value. They can expressed as:

$$Acq_{LCB}(x) = k\sigma_Q(x) - \mu_Q(x) \tag{21}$$

$$Acq_{UCB}(x) = k\sigma_Q(x) + \mu_Q(x) \tag{22}$$

where μ_Q is the posterior mean, σ_Q is the posterior standard deviation, and $k \geq 0$.

The PI is to maximize the probability of improvement over the minimum value of all observation points. When using the PI method to find the next point, it is a pure exploitation process compared to balanced "exploitation" and "exploration". In order to increase its "exploration" ability, the parameter ξ is added in the equation. The PI can be expressed as:

$$\begin{aligned} Acq_{PI}(x) &= P_Q\left(f(x) < f\left(x^+\right) - \xi\right) \\ &= \Phi\left(\frac{f\left(x^+\right) - \mu_Q(x) - \xi}{\sigma_Q(x)}\right) \end{aligned} \tag{23}$$

where $\Phi(\cdot)$ is the cumulative distribution function of the standard normal, x^+ is the point with the minimum f value among all observation points, and ξ is a trade-off parameter slightly greater than 0.

The EI method considers not only the possibility of improvement, but also the room for improvement. So the "exploration" capability of the EI method is more than the PI method. The EI can be expressed as:

$$\begin{aligned} Acq_{EI}(x) &= E_Q\left(max\left(0, f\left(x^+\right) - f(x) - \xi\right)\right) \\ &= \begin{cases} \left(f\left(x^+\right) - \mu_Q(x) - \xi\right)\Phi(Z) + \sigma_Q(x)\phi(Z), \\ \qquad \sigma_Q(x) > 0 \\ 0, \quad \sigma_Q(x) = 0 \end{cases} \end{aligned} \tag{24}$$

where $\phi(\cdot)$ is probability density function of the standard normal, and $Z = \left(f\left(x^+\right) - \mu_Q(x) - \xi\right) / \sigma_Q(x)$.

To further compare the three acquisition functions, the GP with three acquisition functions is applied to find $x_{\text{best}} = \text{argmin}_x y(x)$ in Equation (25) as:

$$y = 2 - [e^{-(x-2)^2} + e^{\frac{-(x-6)^2}{10}} + \frac{1}{x^2+1}] \tag{25}$$

The GP prediction process with the three acquisition functions is shown in Fig. 2. The three columns (a), (b), and (c) correspond to the three acquisition functions LCB, PI, and EI. The initial observation points are set at $x = -1$ and $x = 7$, and the subsequent 7 observation points are obtained according to the three acquisition functions, corresponding to graphs Fig. 2(a)-2 to Fig. 2 (a)-8, Fig. 2(b)-2 to Fig. 2(b)-8, and Fig. 2(c)-2 to Fig. 2 (c)-8. Each graph in Fig. 2 contains two parts: the GP (upper) and the acquisition function curve (lower). The red solid line in the upper part is the objective function y, the black dotted line is the mean of the Gaussian posterior distribution, and the green shaded area represents the 95% confidence interval of the predicted distribution.

Comparing the search for x_{best} point process of the three acquisition functions, the methods LCB and PI are all "sink" in the local minimum. However, there is a difference between the two methods. The PI method can jump out to search for other ranges after several times around the local minimum, while the LCB method is always search for the x_{best} point around the local minimum. Compared with the first two methods, the results of the PI method are ideal. The Gaussian process with 9 observation points selected by PI method can find the best point.

B. DEEP CONVOLUTIONAL NEURAL NETWORK

The DCNN [30] is a stack by several CNN layers. The CNN is derived from the neocognitron model proposed by Japanese scholar Fukushima in 1980 [31]. The development of neocognitron model was inspired by the animal's visual cortex, which consists of the S-layer (consist of simple cells) and C-layer (consist of complex cells). The theory of the S-layer and C-layer continue to evolve into convolution layer and pooling layer in the CNN. In the next 20 years, however, CNN has not been greatly developed due to the limitations of computing power at that time and the rise of algorithms such as HMM and support vector machine (SVM).

Until the upsurge of deep learning research caused by Hinton [32] in 2006, the CNN has regained widespread attention. And with the rapid development of computing devices, the recognition accuracy of CNN method on large-scale visuals far exceeds other methods. The algorithm based on CNN has won many awards in the ImageNet large scale visual recognition challenge (ILSVRC) since 2012, such as AlexNet, ZFNet, VGGNet, GoogLeNet, and ResNet. The CNN can use two-dimensional data as input, and also has the characteristics of weight sharing. This paper applies CNN to fuse multi-sensor signals to predict the RUL of mechanical equipment. The CNN typically

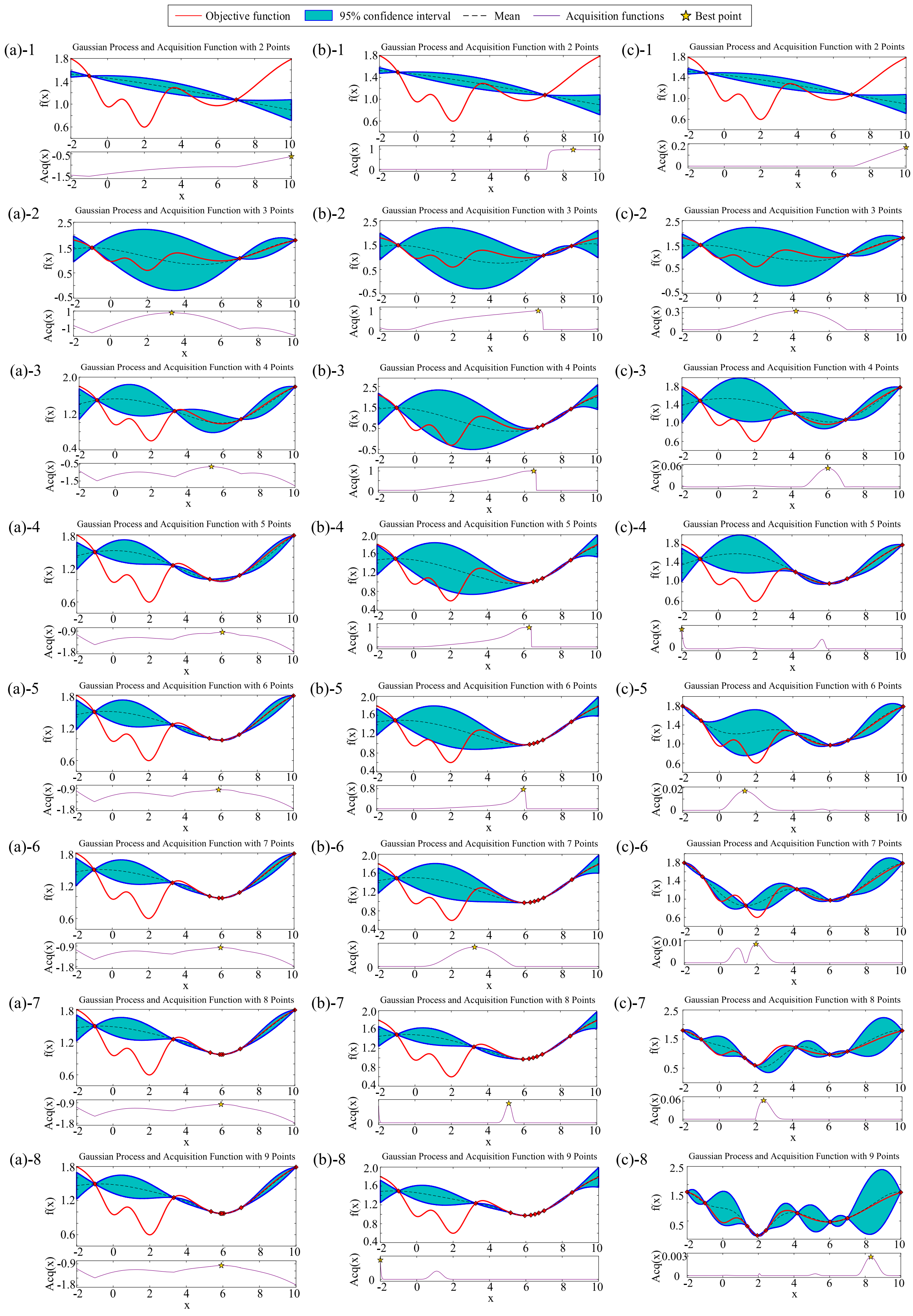

FIGURE 2. **Influence of acquisition function on Gaussian process: (a) lower confidence bound, (b) probability of improvement, and (c) excepted improvement.**

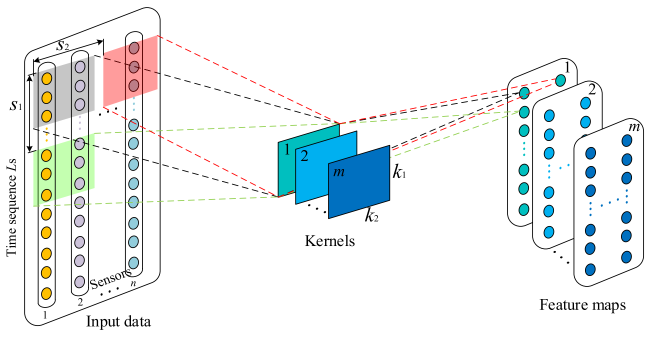

FIGURE 3. Operation of 2D-convolution.

includes convolution operation, activation operation, pooling operation, and dropout operation for overfitting prevention.

1) CONVOLUTIONAL OPERATION AND ACTIVATION OPERATION

The convolution operation [33] consists of input data, convolution kernels, and the resulting feature maps. Fig. 3 shows a two-dimensional (2D) convolution operation in which the input data is 2D data consisting of signals collected by n sensors.

The convolution filter extracts multiple matrixes by sliding over the input data. The size of the data extracted each time by convolutional filter is the same as the size of the convolution kernel. The three shaded portions in the input data are the three adjacent data extractions of the sliding convolutional filter. The element-wise multiplication was performed between the each data matrix extracted by the convolution filter and the convolution kernel. Then all the elements in the result are summed and plus an offset to obtain an element in feature map. As the convolutional filter slides continuously to extract the data matrix, a complete feature map can be obtained. By repeating the above convolution operation on the m convolution kernels, m feature maps can be obtained.

As shown in Fig. 3, the vertical axis of the input data is the length of the time sequence L_s, and the horizontal axis is signals collected by n sensors. The convolution filter and the convolution kernel are the same size, i.e., filter_size = kernel_size = $[k_1, k_2]$. The sliding step of the convolution filter is $[S_1, S_2]$. The number of convolution kernels and the number of feature maps are equal to m. The size of the feature map is $[(L_s - k_1)/S_1 + 1, (n - k_2)/S_2 + 1]$. As described above, it is known that the larger the sliding step of the convolution filter, the smaller the feature map obtained. In order to increase the size of feature map and extract the edge information of the input data, the input edge padding process is performed. If the padding dimension is p, the feature map size obtained after data edge padding is $[(L_s - k_1 + 2p)/S_1 + 1, (n - k_2 + 2p)/S_2 + 1]$. Therefore, the obtained feature map size can be adjusted by the padding dimension p. It should be noted that the obtained feature map size should be an integer. The data used for padding is usually 0, which is called zero-padding. Other data can also be used for padding the input data. The mathematical

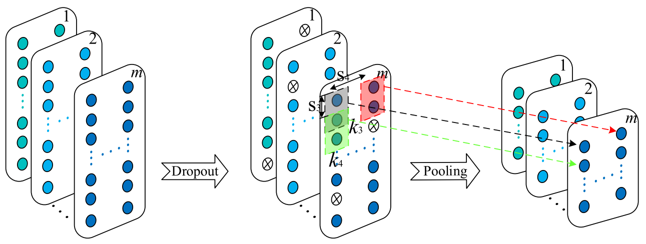

FIGURE 4. Operations of dropout layer and pooling layer.

expression of the convolution operation and the activation operation are as follows:

$$h_{ij}^{m} = sum\left(\boldsymbol{W}_m \odot \boldsymbol{F}_{ij}^{c}\right) + b_m \tag{26}$$

$$y_{ij}^{m} = \varphi(h_{ij}^{m}) \tag{27}$$

where $\boldsymbol{W}_m$ is the m-th kernel matrix, $\boldsymbol{F}_{ij}^{c}$ is the data matrix extracted by the sliding convolutional filter, $\odot$ is the element-wise multiplication, b_m is the offset of the m-th convolution kernel, h_{ij}^{m} is the m-th feature map, i and j are the stride of the convolutional filter in the vertical and horizontal directions, sum(&) is a process to sum all of elements in &, $\varphi(\ )$ is an activation function, and y_{ij}^{m} is the output of activation.

2) DROPOUT OPERATION AND POOLING LAYER

The purpose of dropout operation [34] for neurons in the hidden layer is to avoid the network overfitting. It randomly makes the hidden layer neurons to zero based on the dropout probability d_p. When the dropout operation is not performed, all parameters of the network are fine-tuned at each epoch of training. Multiple iterations training under the same network structure resulted in a very low training loss, but the testing results are usually not as expected. By randomly dropout part of the neurons in the hidden layer, the numbers of the neurons involved in each training epoch are different. The dropout layer is usually placed after the convolution layer. As shown in Fig. 4, the output of the activation function is randomly zeroed according to the dropout probability d_p. The role of the dropout layer is to randomly reset some values in the feature map to zero. The symbol $\otimes$ in Fig. 4 represents the neuron reset to zero.

The mathematical expression of the dropout operation is shown in Equation (28). The dropout operation is only used during the training process. However, all neurons are active when the network is used for testing. Therefore, the coefficient $1/(1-d_p)$ was used to correct the difference between training and testing in dropout operation, as shown in Equation (29).

$$\boldsymbol{R} = rand\left(size\left(\boldsymbol{Y}\right)\right) > d_p \tag{28}$$

$$\tilde{\boldsymbol{Y}} = (\boldsymbol{R} \odot \boldsymbol{Y})/(1-d_p) \tag{29}$$

where *rand*( ) function randomly generated numbers between 0 to 1, *size*( ) extracts the dimensions of the matrix $\boldsymbol{Y}$, $\boldsymbol{R}$ is dropout mask containing only 0 and 1, $\tilde{\boldsymbol{Y}}$ is the output of dropout layer.

Following the dropout layer, the pooling layer [35] is used to reduce the dimension of the data and extract the data characteristics. The pooling filter size is [k_3, k_4] and the sliding step of the pooling filter is [S_3, S_4]. Unlike the convolution operation, only the data extracted by the filter itself performs some pooling processing. Commonly used pooling operations are maximum pooling (*Max_pooling*) and average pooling (*Average_pooling*). The *Max_pooling* selects the maximum value of the data extracted by the filter, and the *Average_pooling* averages all the data extracted by the filter. So the number of output elements is equal to the number of filters in the pooling layer.

The mathematical expressions of the *Max_pooling* operation and *Average_pooling* operation are as follow:

$$y_{ij}^{p} = Max\_pooling(\boldsymbol{F}_{ij}^{p}) \tag{30}$$

$$y_{ij}^{p} = Average\_pooling(\boldsymbol{F}_{ij}^{p}) \tag{31}$$

where $\boldsymbol{F}_{ij}^{p}$ is the data matrix extracted by the sliding pooling filter, y_{ij}^{p} is the p-th output of pooling layer, i and j are the stride of the pooling filter in the vertical and horizontal directions.

C. ADAPTIVE BATCH NORMALIZATION

A DL based RUL prediction model can be developed based only on data. The dataset used to develop a model with different working conditions and fault types is called the data domain (DD). The prediction models developed in different DDs are often not universal to each other. In order to make the developed prediction model have a better adaptability to various DDs, this paper applies the AdaBN algorithm [36]. AdaBN is a novel transfer learning strategy based on batch normalization (BN). A BN layer normalizes each input channel across a mini-batch. It is usually placed between the convolution operation and the activation operation. The BN layer can speed up the network training process and reduce the sensitivity of the convolution operation on the output data. In the training process, all the samples are divided into several mini-batches for separate training. If the sample size is represented by s and the number of samples included in each mini-batch is represented by b, then the number of batches n_b is equal to s/b. As shown in Equation (32), the BN layer first normalizes the output of each channel by subtracting the mean of the mini-batch and dividing by standard deviation of the mini-batch. However, the normalization results are trapped in the linear activation interval of the sigmoid and tanh activation functions. Therefore, the normalized results shift by the learnable offset β^c and scale by the learnable scale factor γ^c. Moreover, when $\beta^c = \mu(\boldsymbol{X}_{1:b}^{c})$ and $\gamma^c = \sigma^2\left(\boldsymbol{X}_{1:b}^{c}\right)$, it is equivalent to keeping the original state of the input data $\boldsymbol{X}_j^c$ unchanged.

$$\hat{\boldsymbol{X}}_j^c = \frac{\boldsymbol{X}_j^c - \mu(\boldsymbol{X}_{1:b}^{c})}{\sqrt{\sigma^2\left(\boldsymbol{X}_{1:b}^{c}\right) + \epsilon}} \tag{32}$$

$$\boldsymbol{Y}_j^c = \gamma^c * \hat{\boldsymbol{X}}_j^c + \beta^c \tag{33}$$

where $\boldsymbol{x}_j^c$ is j-th ($j = 1, \ldots, b$) input in a mini-batch of channel c, $\mu(\boldsymbol{X}_{1:b}^{c})$ and $\sigma^2\left(\boldsymbol{X}_{1:b}^{c}\right)$ are the mean and variance of one mini-batch in channel c, ϵ is a very small positive number for improving numerical stability when $\sigma^2\left(\boldsymbol{X}_{1:b}^{c}\right)$ is very small, and γ^c, β^c are scale factor and offset.

The test data is not batch-processed and input into the network at one time. Therefore, μ and σ^2 in Equation (32) are replaced by the μ_{test} and σ_{test}^2 as shown in Equations (34-35).

$$\mu_{test} = E(\mu_{1:n_b}) \tag{34}$$

$$\sigma_{test}^2 = \frac{n_b}{n_b - 1} E(\sigma_{1:n_b}^2) \tag{35}$$

where n_b is the number of batches in training process, and E( ) is the average operation.

When the prediction DD is different but similar to the training DD, the transfer learning method is commonly used to retrain the network. The traditional transfer learning method retrains part of the weights and bias in the network to adapt to the different DDs. In this way, not a large amount of parameters need to be retrained. Only the retrained layers in the network play a predictive role. The AdaBN method applied in this paper keeps the weights and biases of the network unchanged, and only retrains the scale factor γ^c and offset β^c in the BN layer. Of course, μ and σ^2 should also be replaced with μ_{target} and σ_{target}^2.

$$\hat{\boldsymbol{X}}_j^c = \frac{\boldsymbol{X}_j^c - \mu_{target}}{\sqrt{\sigma_{target}^2 + \epsilon}} \tag{36}$$

$$\boldsymbol{Y}_j^c = \gamma_{retrain}^c * \hat{\boldsymbol{X}}_j^c + \beta_{retrain}^c \tag{37}$$

where μ_{target} and σ_{target}^2 are mean and variance of target domain, $\gamma_{\text{retrain}}^c$ and β_{retrain}^c are retrained scale factor and offset with target data.

III. THE PROPOSED METHOD

In this paper, the proposed RUL prediction method based on DCNN combined with Bayesian optimization and AdaBN algorithm is explained. The Bayesian optimization method is used to select the optimal network structure and training hyperparameters. The AdaBN algorithm is used to improve the adaptability of the network in multiple data domains. The challenge in combining Bayesian optimization and DCNN is that the network testing results should be used as the basis for finding new observation points for Bayesian optimization. However, the test results of the prediction models trained multiple times with the same hyperparameters are not the same. Therefore, a Gaussian process fit with 'noise' is used to adapt to this situation. The combination with the AdaBN algorithm needs to add several BN units in the DCNN. In addition, when processing different test domains, the parameter scale factor and offset in the BN unit must be fine-tuned.

The hyperparameters are parameters set during network training such as learning rate, batchsize, momentum, etc. The hyperparameters is difficult to select and has a large impact on the prediction results. It is usually based on the experience

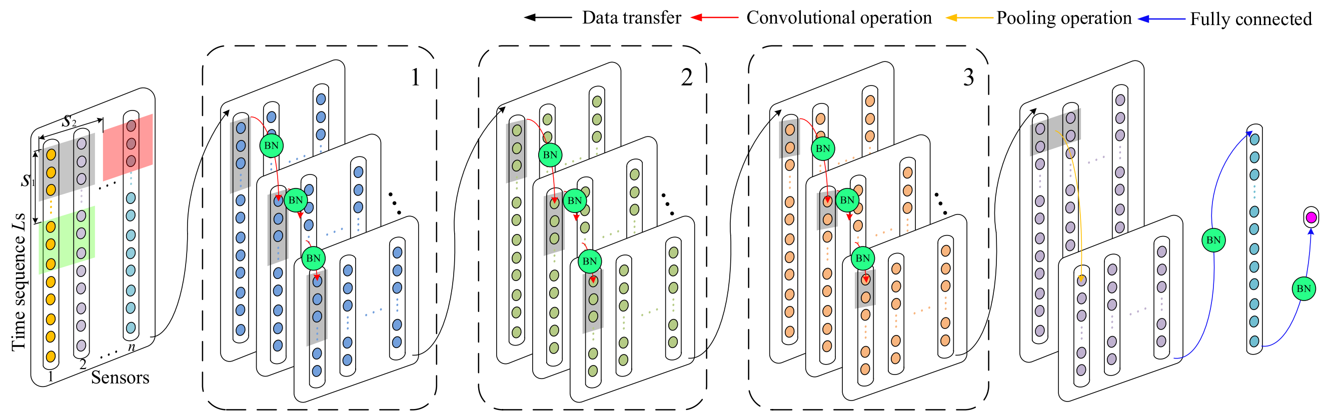

FIGURE 5. Framework of the Bayesian optimization AdaBN-DCNN RUL prediction model with uncertain structures.

TABLE 2. Hyperparameters selected by Bayesian optimization method.

Hyperparameters	Name	Range
Structural parameter	Network depth	[1, 3]
Training parameters	Initial learning rate	[5e-4, 1e-2]
	Batchsize	[200, 1000]
	Momentum	[0.3, 0.95]
	L2 Regularization	[1e-10, 1e-2]

of the researcher to select the best hyperparameters through multiple trials. Table 2 shows the parameters selected by Bayesian optimization method, including structural parameter and training parameters. The range of parameters is chosen empirically. The Bayesian algorithm selects the parameters with the best prediction result through multiple iterations within the set range.

The structural parameter 'network depth' will be introduced below in conjunction with the framework graph of the proposed method. This paper uses a piecewise learning rate. First set an initial learning rate, then the learning rate gradually decreases by the amount determined as a certain number of training epochs multiplying with a certain factor. The number of epochs for dropping the learning rate is represent by 'learning rate drop period', and the factor for dropping the learning rate is represent by 'learning rate drop factor'. The learning rate drop period and learning rate drop factor are set to 10 and 0.5 respectively. The training samples will be divided into several mini-batches for training. The sample size contained in each batch is represented by batchsize. The batchsize represents an integer number of samples. The standard gradient descent (SGD) algorithm with momentum is used to updates the network parameters (weights and biases) and minimizes the loss function. The SGD algorithm can oscillate along the steepest descending path to the optimum, and the momentum term can reduce this oscillation. Adding the L2 regularization term for the weights is one way to reduce over-fitting.

Fig. 5 shows the framework of the Bayesian optimization AdaBN-DCNN RUL prediction model with uncertain structures. The prediction method proposed in this paper is based on DCNN, which includes several convolutional layers, one pooling layer and two fully connected layers. The uncertain structure in the prediction model is determined by 3 dotted boxes. The number of dotted boxes represents the 'network depth' in Table 2. The same number of convolutional layers contain in the three dotted boxes.

And the number of dashed boxes that make up the prediction model is determined by Bayesian optimization. In order to improve the network's ability to adapt to multiple DDs, BN units have been added in the convolutional layer and the fully connected layer. When dealing with different predicted DDs, only the green BN unit in Fig. 5 needs to be retrained to make a better prediction result. The filters of multiple convolutional layers in the same dashed boxes have the same size, stride and numbers. The filter size in the three dashed boxes are [6 1], [4 1] and [2 1] respectively. All the filters have the same stride [2 1]. The same number of filters is used for all the convolution layers in the same dashed box. The initial number of filters can be determined by Equation (38). The number of filters used for the convolution layer in the three dashed boxes are $\mathrm{Num}_{\mathrm{Filters}}$, $2 \times \mathrm{Num}_{\mathrm{Filters}}$, and $3 \times \mathrm{Num}_{\mathrm{Filters}}$ respectively.

$$Num_{Filters} = round(10/\sqrt{n_d}) \tag{38}$$

where n_d is the 'Network depth', *round*( ) is a function round to nearest integer, and $\mathrm{Num}_{\mathrm{Filters}}$ is the initial number of filters.

There is a pooling layer and two fully connected layers after the convolutional layers. The *Average_pooling* operation is used in the pooling layer. The pooling filter size is [1 2], and the stride of the pooling filter is [1 1]. The number of neurons in the two fully connected layers is 30 and 1 respectively. The activation function used in the prediction network is ReLU. The activation function is not shown in Fig. 5, and it should be placed behind the green BN unit. The output of the last fully connected layers is the predicted RUL.

Table 3 shows the overall flow of the proposed RUL prediction method. The purpose of the proposed method is

TABLE 3. An overall procedure of the proposed RUL prediction method.

```
Algorithm 2: The proposed method
Purpose: Construct a prediction model with self-optimizing structure,
         hyperparameter selection, and domain adaptability.
Step 1. Data preparation:
    ● Sliding time window processes training and test data into short
      segments of [30, 14].
    ● Normalize training and test data with $z$-score.
    ● Save the processed training data $x_{\text{train}}$ and test data $x_{\text{test}}$.
Step 2. AdaBN-DCNN model construction:
    ● Set the structure of AdaBN-DCNN model as shown in Fig.5.
    ● Input training data and hyperparameters into the model for
      training. The types and ranges of the hyperparameters are
      shown in Table 2.
    ● The trained AdaBN-DCNN model can be represented by
      $f_{N_d,l_r,B_s,M_o,L2}$, where $N_d$, $l_r$, $B_s$, $M_o$, $L2$ are the hyperparameters:
      network depth, initial learning rate, batchsize, momentum, and
      L2 regularization. Then the predicted error $E$ can be expressed
      as $E = f_{N_d,l_r,B_s,M_o,L2}(x_{\text{test}})$.
Step 3. Search for the best set of hyperparameters:
    ● Randomly select one set of hyperparameters to train the
      AdaBN-DCNN model. Compute the test error $E$.
    ● Perform Gaussian process regression and search for the next
      observation (A new set of hyperparameters need to be verified)
      based on acquisition function.
    ● Input the new set of hyperparameters into the AdaBN-DCNN
      model for training and compute a new test error.
    ● Repeat the above two steps until the set number of
      optimization steps is reached.
    ● Finally, record the best test error and corresponding
      hyperparameters.
Step 4. Strategies for the new test data domain $x'_{\text{test}}$:
    ● The best hyperparameters have been selected in Step 3 to train
      the prediction model constructed in Step 2.
    ● When the test data domain changes, it is only necessary to
      apply the corresponding $x'_{\text{train}}$ to retrain the scale factor and
      offset in the BN unit. No other parameters need to be changed
      in the model.
Output: A prediction model with hyperparameters optimized and the
        domain adaptability enhanced.
```

to construct a prediction model with self-optimizing structure and hyperparameter selection. It improves domain adaptability of the model. The first step is to segment and normalize the training and test data. Step 2 builds an AdaBN-DCNN model for prediction. The function f between various hyperparameters and test errors is also developed. Step 3 is the process of searching for the best hyperparameter set using Bayesian optimization. Step 4 is to use AdaBN strategy to improve prediction accuracy with changing test data domains.

IV. VALIDATION OF THE PROPOSED METHOD

A. C-MAPSS DATASET DESCRIPTION

The simulated turbofan engine run to failure data was used to validation the proposed prediction model. The simulated data was produced using a model based simulation program C-MAPSS developed by NASA [37]. This section provides a detailed description of 5 parts: simulated signal selection, time window (TW) processing, data normalization, RUL function correction, and model evaluation method. As shown in Fig. 6, the structure of the simulated turbofan mainly consists of 5 parts: fan, low pressure compressor (LPC),

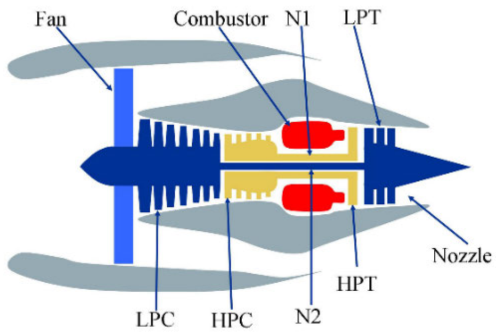

FIGURE 6. A simplified diagram of the simulation engine in C-MAPSS.

TABLE 4. Description of the C-MAPSS dataset.

Dataset Contents	Sub-datasets			
	FD001	FD002	FD003	FD004
Engines in training set	100	260	100	249
Engines in test set	100	259	100	248
Max/min cycles for training	362/128	378/128	525/145	543/128
Max/min cycles for test	303/31	367/21	475/38	486/19
Operating condition	1	6	1	6
Fault modes	1	1	2	2
TW length	30	21	36	18
Training samples	17731	48559	21220	57016
Test samples	100	259	100	248

high pressure compressor (HPC), combustor, high pressure turbine (HPT), and low pressure turbine (LPT). Symbols N1 and N2 in Fig. 6 represent the core shaft and the fan shaft, respectively.

The C-MAPSS datasets contains multiple sets of run to failure data from different engine states. It is divided into 4 sub-datasets according to the simulated operating conditions and fault modes. Each sub-dataset contains independent training data and test data which consists of several sets of data from different engine run to failure health conditions. For example, FD001 contains 100 sets of training engine data and 100 sets of test engine data. In order to test all the data in the test dataset, the TW length should be less than or equal to the minimum number of cycles in the test dataset. More details on the C-MAPSS dataset are given in Table 4.

The description of the 21 collected engine simulation sensor outputs is provided in Table 5. As the operating state of the engine changes, some of the collected data show a significant trend of increasing (↑) or decreasing (↓), while others show a fluctuating trend (~). In order to meet the prediction requirements, only 14 simulation output signals with a significant trend were selected as inputs to the predictive model.

14 signals with regular trends in Table 5 were selected to evaluate the RUL of the engine. The RUL of the engine is measured in cycles. Each data point in each cycle of the engine contains 14 features. Normally, one would use the 14 features as inputs to predict the RUL. Since the signals don't change consistently with RUL of the engine and the time series data cannot directly fed into a CNN, the method proposed uses a period of time data to predict the RUL of the

TABLE 5. 21 sensor outputs of the simulation engine running.

#	Symbol	Description	Units	Trend
1	T2	Total Temperature at fan inlet	°R	~
2	T24	Total temperature at LPC outlet	°R	↑
3	T30	Total temperature at HPC outlet	°R	↑
4	T50	Total temperature LPT outlet	°R	↑
5	P2	Pressure at fan inlet	psia	~
6	P15	Total pressure in bypass-duct	psia	~
7	P30	Total pressure at HPC outlet	psia	↓
8	Nf	Physical fan speed	rpm	↑
9	Nc	Physical core speed	rpm	↑
10	Epr	Engine pressure ratio	--	~
11	Ps30	Static pressure at HPC outlet	psia	↑
12	Phi	Ratio of fuel flow to Ps30	pps/psi	↓
13	NRf	Corrected fan speed	rpm	↑
14	NRc	Corrected core speed	rpm	↓
15	BPR	Bypass ratio	--	↑
16	farB	Burner fuel-air ratio	--	~
17	htBleed	Bleed enthalpy	--	↑
18	NF_dmd	Demanded fan speed	rpm	~
19	PCNR_d md	Demanded corrected fan speed	rpm	~
20	W31	HPT coolant bleed	lbm/s	↓
21	W32	LPT coolant bleed	lbm/s	↓

engine as the RUL of the last time point in this period. The sliding TW method was used to cut an entire time series data into several segments. The time series length is T_s, the TW length is L_{tw}, and the sliding step of the TW is S_l. Then the obtained number of data segments is $(T_s - L_{tw})/S_l + 1$.

As a result of the pre-processing, 14 engine-related features were generated from the 14 selected sensor output signals. The values of these features vary from zero to hundreds. In order to use these features uniformly as input to the predictive model, it is necessary to normalize the feature values. In this paper, the z-score normalization processing was applied to process each feature separately, as shown in Equation (39):

$$\boldsymbol{y}_n = (\boldsymbol{x}_n - \mu_x)/\sigma_x \tag{39}$$

where $\boldsymbol{x}_n$ is the n-th feature vector, μ_x is the average of feature vector $\boldsymbol{x}_n$, σ_x is the standard deviation of feature vector $\boldsymbol{x}_n$, and $\boldsymbol{y}_n$ is the normalized data.

The first engine of the FD001 training set contains 192 cycles. The selected 14 engine related features were normalized as shown in Fig. 7(a). It can be seen that the 14 signals either increase or decrease with engine degradation. The predictive model predicts the RUL of the engine based on changes in parameters during engine degradation. However, it can be seen from Fig. 7 that the features remain relatively unchanged at the beginning of the engine operation. Based on this observation, the standard output of the prediction model was modified. The commonly used linear RUL function was replaced by the piecewise linear RUL function. According to the literature [38], the maximum service life of the engine is set to 125. As shown in Fig. 7(b), a piecewise linear RUL function is obtained by replacing RUL > 125 in the linear RUL function with 125.

To measure the RUL prediction accuracy, both late prediction and early prediction errors have to be considered.

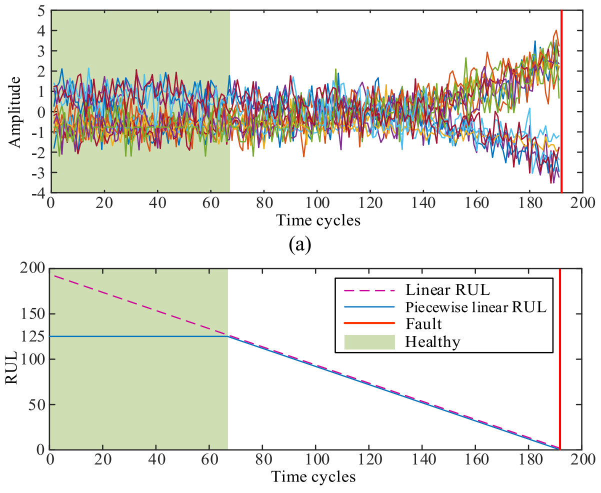

FIGURE 7. Engine #1 in FD001 sub-dataset: (a) normalized 14 signals and (b) piecewise linear RUL function.

When the predicted RUL is greater than the actual RUL, it is called late prediction, and the opposite is called early prediction. In order to evaluate the predictive ability of the model, two commonly used evaluation methods are adopted in this paper, as shown in Equations (40) and (41). Comparing the two evaluation methods, it can be found that E_{RMSE} in Equation (40) has the same penalty for both the late prediction and the early prediction, while E_{score} in Equation (41) has a greater penalty for the late prediction.

$$E_{RMSE} = \sqrt{\left(\sum\nolimits_{i=1}^{m} (y_i^p - y_i^a)^2\right)\Big/ m} \tag{40}$$

$$E_{score} = \sum\nolimits_{i=1}^{m} d_i,\ d_i = \begin{cases} e^{-(y_i^p - y_i^a)/13}, & y_i^p - y_i^a < 0 \\ e^{-(y_i^p - y_i^a)/10}, & y_i^p - y_i^a \geq 0 \end{cases} \tag{41}$$

where E_{RMSE} is the root mean square error of the prediction result, E_{score} is a prediction result evaluation method, y_i^p is the predicted RUL of i-th test engine, y_i^a is the actual RUL of i-th test engine, and m is the number of test engines.

B. RESULTS AND ANALYSIS

1) PREDICTION RESULTS WITH BAYESIAN OPTIMIZATION

The advantage of the proposed method is that it can optimize the structure and select hyperparameters by itself. Therefore, only the range of the parameters needs to be determined during network training, as shown in Table 2. As shown in Fig. 5, the network includes three types of layers: convolutional layer, pooling layer, and fully connected layer. The filter sizes of the convolutional layers in the three dashed boxes are [6 1], [4 1] and [2 1], respectively. All the filters have the same stride [2 1]. The pooling filter size is [1 2], and the stride of the pooling filter is [1 1]. The number of neurons in the two fully connected layers are 30 and 1. The standard gradient descent (SGD) algorithm with momentum was used to update the network parameters. The maximum number of training epochs was set to 40. The number of epochs for dropping the learning rate was represent by 'learning rate drop period',

TABLE 6. **Bayesian optimization for multiple iterations to search for the best parameters in FD001.**

#	Evaluation result	Running time /s	E_{RMSE}	Best E_{RMSE}	Network Depth	Initial LR	Momentum	Batchsize	L2 Regularization
1	**Best**	**149.37**	**13.51**	**13.51**	**2**	**0.001412**	**0.3021**	**287**	**0.000696219**
2	**Best**	**117.69**	**12.61**	**12.61**	**2**	**0.001311**	**0.3490**	**777**	**1.79E-08**
3	Accept	144.06	13.15	12.61	3	0.006729	0.5768	330	9.49E-06
4	Accept	168.74	14.35	12.61	1	0.001587	0.9481	676	5.04E-05
5	Accept	133.31	12.83	12.61	3	0.007588	0.3888	394	1.68E-08
6	**Best**	**120.06**	**12.09**	**12.09**	**2**	**0.004079**	**0.3795**	**622**	**2.07E-08**
7	Accept	122.87	13.11	12.09	2	0.000529	0.6874	512	2.73E-08
8	Accept	169.92	13.42	12.09	1	0.000505	0.3009	602	3.99E-08
9	Accept	130.34	12.67	12.09	2	0.009383	0.6794	554	7.56E-09
10	Accept	133.97	12.91	12.09	2	0.004572	0.7831	587	4.58E-08
11	Accept	134.41	13.79	12.09	2	0.006193	0.3060	273	2.59E-09
12	Accept	111.61	12.82	12.09	3	0.008734	0.3084	641	0.000222756
13	**Best**	**121.52**	**11.94**	**11.94**	**2**	**0.008090**	**0.3450**	**642**	**0.001895096**
14	Accept	117.74	12.59	11.94	2	0.009633	0.3105	622	6.35E-08
15	Accept	126.44	12.44	11.94	2	0.002411	0.4293	667	0.001205983
16	Accept	121.82	13.04	11.94	2	0.008564	0.3062	659	3.56E-07
17	Accept	123.78	12.67	11.94	2	0.009031	0.3934	581	0.004004175
18	Accept	128.08	12.76	11.94	2	0.000913	0.4503	686	8.24E-10
19	Accept	221.45	15.74	11.94	1	0.000707	0.3167	204	1.08E-10
20	Accept	117.77	13.29	11.94	3	0.002011	0.9499	799	4.70E-07
21	Accept	168.51	13.21	11.94	1	0.006643	0.3016	800	4.69E-07
22	Accept	121.42	13.05	11.94	3	0.001224	0.3029	800	2.20E-07
23	Accept	160.06	14.24	11.94	3	0.004702	0.3030	200	6.09E-06
24	Accept	218.06	16.34	11.94	1	0.000703	0.9500	201	1.51E-10
25	Accept	118.24	12.74	11.94	3	0.000566	0.9489	538	2.97E-10
26	Accept	125.72	12.70	11.94	2	0.008057	0.9360	800	0.001878173
27	Error	152.69	None	11.94	2	0.005110	0.9475	200	0.001273025
28	Accept	160.85	16.06	11.94	2	0.001560	0.9477	201	1.52E-10
29	Accept	114.40	13.13	11.94	3	0.001073	0.3020	527	1.69E-07
30	Accept	108.93	12.47	11.94	3	0.000634	0.6875	647	0.008517568

and the factor for dropping the learning rate was represent by ‘learning rate drop factor’. The learning rate drop period and learning rate drop factor were set to 10 and 0.5, respectively.

The results of predicting FD001 sub-dataset of the C-MAPSS using the proposed prediction model are provided in Table 6. The information for the 30 iterations in the table include: evaluation result, running time, E_{RMSE}, best E_{RMSE}, and selected 5 hyperparameters. There are three measures for the evaluation results: ‘Best’, ‘Accept’, and ‘Error’. The evaluation results are based on E_{RMSE}. When the obtained E_{RMSE} is the current minimum, the measure of the evaluation results for this iteration is ‘Best’. When the obtained E_{RMSE} is not the minimum value and the result of this iteration is accepted by Bayesian optimization, the measure of the evaluation results for this iteration is ‘Accept’. When the result cannot be used for the subsequent Bayesian optimization, the measure of the evaluation results is ‘Error’. E_{RMSE} is the evaluation result of the model tested by the test dataset. Smaller test E_{RMSE} values indicate that the corresponding model has better prediction capacity. ‘Best E_{RMSE}’ shows the best E_{RMSE} obtained by the existing iterations. The 5 parameters, such as network depth and initial learning rate (LR) etc., were selected in the range by the Bayesian optimization.

The proposed prediction method was used on the 4 sub-datasets of C-MAPSS, and the results obtained are shown in Table 7. It contains the test E_{RMSE} result, the running time and the hyperparameters corresponding to the best E_{RMSE}. It can be seen from Table 4 that the time window length of the 4 datasets are different. The obtained sample size is also different. Therefore, the sliding step of the CNN filter for different sub-dataset is different. The sliding step of the FD001 and FD002 datasets is [2, 1], the sliding step of FD003 is mixed with [2, 1] and [1, 1], and the sliding step of FD004 is [1, 1]. Therefore, the running time of the proposed method on the 4 sub-datasets is also quite different as shown in Table 7.

Fig. 8 shows the prediction results of the prediction method in the FD001 dataset. Fig. 8(a) shows the prediction RUL curve and the actual RUL curve for 100 test engine units in FD001. The prediction capability of the network can be roughly seen from Fig. 8(a). In order to display the prediction results more intuitively, the 100 prediction engine units were sorted by the actual RUL as shown in Fig. 8(b). The red line is the sorted actual RUL, the black triangle label is the distribution of predicted RUL, and the colored area is the error band. The prediction error of the engines can be directly observed by the distribution of prediction RUL in the error band. The prediction error distribution histogram of the FD001 test sub-dataset is shown in Fig. 8(c). It can be seen from Fig. 8(c) that the number of engines with a prediction error between [−10, 10] is 69%, and between [−20, 20] is 89%. Similarly, Fig. 9 - Fig.11 show the test results of the FD002, FD003, and FD004 test datasets.

The two measures shown in Equations (40) and (41) were used for evaluating the prediction results. In order to show the prediction capability of the proposed method, the results

TABLE 7. The best parameters selected by the Bayesian optimization for the 4 sub-datasets.

#	Running time /s	E_{RMSE}	Network Depth	Initial LR	Momentum	Batchsize	L2 Regularization
FD001	121.52	11.94	2	0.008090	0.3450	642	0.001895096
FD002	299.91	19.29	2	0.001397	0.9380	783	9.45E-05
FD003	320.42	12.31	3	0.000517	0.5239	799	0.003426757
FD004	1470.90	22.14	1	0.001778	0.8297	800	0.003670858

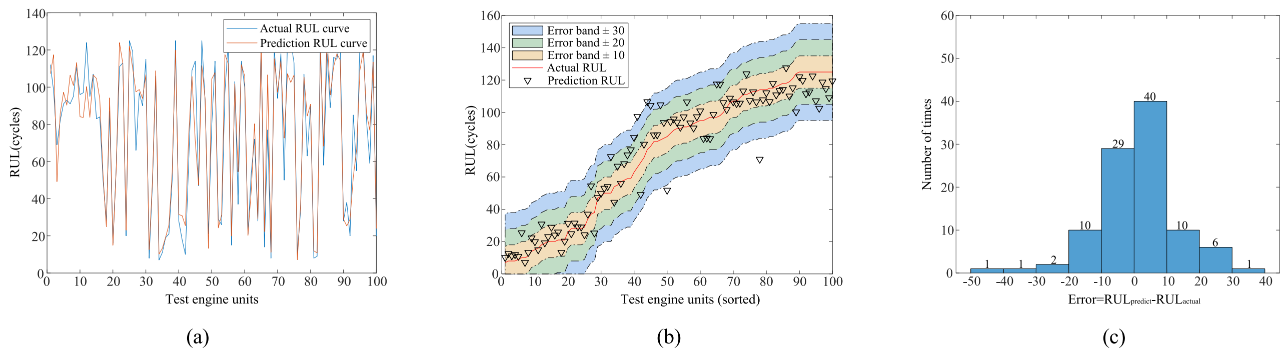

FIGURE 8. Test results of FD001 sub-dataset: (a) comparison of actual RUL curve and prediction RUL curve, (b) prediction results error band, and (c) distribution histogram of prediction error.

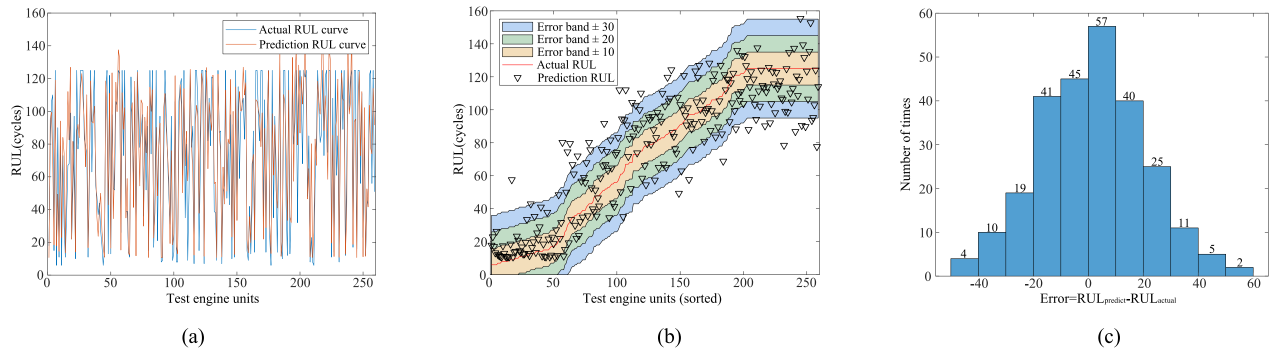

FIGURE 9. Test results of FD002 sub-dataset: (a) comparison of actual RUL curve and prediction RUL curve, (b) prediction results error band, and (c) distribution histogram of prediction error.

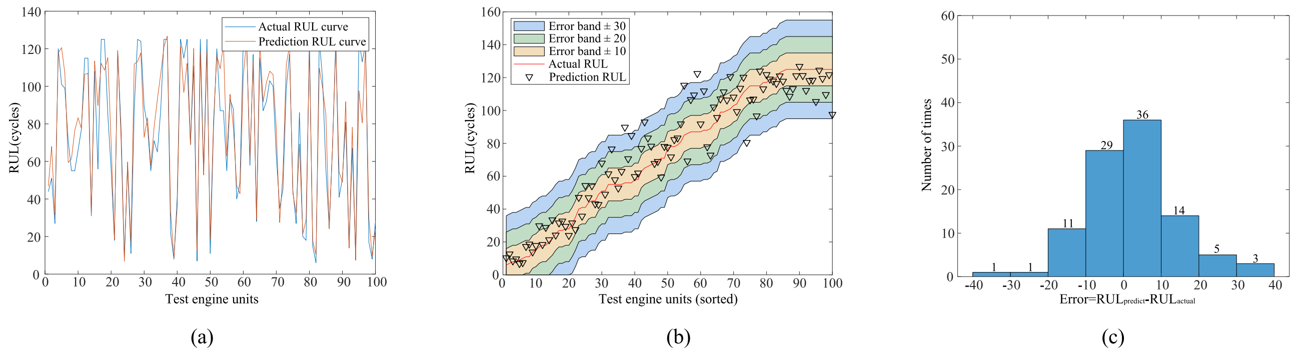

FIGURE 10. Test results of FD003 sub-dataset: (a) comparison of actual RUL curve and prediction RUL curve, (b) prediction results error band, and (c) distribution histogram of prediction error.

of the proposed method along with the prediction methods using C-MAPSS for validation in the past 4 years reported in the literature are presented in Table 8. Although the E_{RMSE} and E_{sorce} evaluation measures are slightly different, both represent a good prediction result when their value is small. In order to highlight the best prediction method, the best results for each comparison are bolded in the table. As shown in the table, the predicted results of the proposed method are the best except for the E_{sorce} result of the FD004 sub-dataset.

2) INFLUENCE OF THE HYPERPARAMETERS ON PREDICTION RESULTS

The Bayesian optimization method searches for the best combination of parameters by continuously adding observation

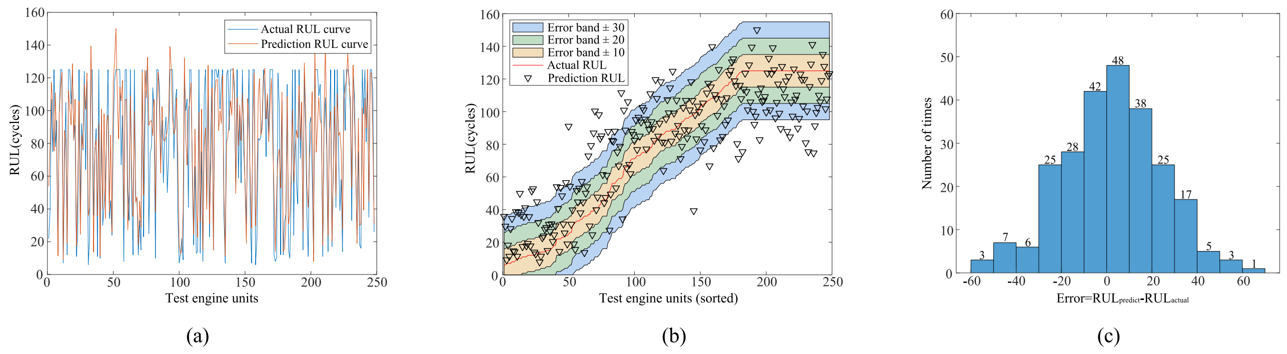

FIGURE 11. Test results of FD004 sub-dataset: (a) comparison of actual RUL curve and prediction RUL curve, (b) prediction results error band, and (c) distribution histogram of prediction error.

TABLE 8. Comparison of the prediction results with other methods.

Methods	Years	FD001		FD002		FD003		FD004	
		E_{RMSE}	E_{sorce}	E_{RMSE}	E_{sorce}	E_{RMSE}	E_{sorce}	E_{RMSE}	E_{sorce}
CNN [39]	2016	18.45	1.29×10^3	30.29	1.36×10^4	19.82	1.60×10^3	29.16	7.89×10^3
LSTM [40]	2017	16.14	3.38×10^2	24.49	4.45×10^3	16.18	8.52×10^2	28.17	5.55×10^3
MODBNE [41]	2017	15.04	3.34×10^2	25.05	5.59×10^3	12.51	4.22×10^2	28.66	6.56×10^3
BLSTM [21]	2018	14.26	-	21.7	-	16.33	-	25.9	-
BiLSTM [38]	2018	13.65	2.95×10^2	23.18	4.13×10^3	13.74	3.17×10^2	24.86	5.43×10^3
DCNN [33]	2018	12.61	2.74×10^2	22.36	1.04×10^5	12.64	2.84×10^2	23.31	1.25×10^5
DAG [42]	2019	11.96	2.29×10^2	20.34	2.73×10^3	12.46	5.35×10^2	22.43	$\mathbf{3.37\times10^3}$
The proposed method	2019	**11.94**	$\mathbf{2.20\times10^2}$	**19.29**	$\mathbf{2.25\times10^3}$	**12.31**	$\mathbf{2.60\times10^2}$	**22.14**	3.63×10^3

points and repeating the Gaussian process. The selection of the next observation points is based on the fitting curve by the Gaussian process. As the number of added observation points increases, the curve fitted by the Gaussian process will approach the actual distribution of the function.

The Gaussian optimization was used to optimize the hyperparameters such as initial learning rate, batchsize, momentum, and L2 regularization respectively. When one hyperparameter is being optimized, the other hyperparameters are set as in Table 7. Fig. 12 shows the Gaussian process for 4 hyperparameters with 30 observation points for the FD001 sub-dataset. The horizontal axis corresponds to the search range of the hyperparameters, and the vertical axis represents the E_{RMSE} value of using the FD001 test dataset for validating the prediction model. The effects of the 4 hyperparameters value on the prediction capacity of the developed model are shown in Fig. 12. The red line in Fig. 12 is the predictive function mean obtained by Bayesian optimization. The 30 blue dots are the 30 observation points for the Gaussian process. The larger black dot is the position of the next observation point selected according to the acquisition function. And the red star point is the point with the lowest function mean. The prediction results by the CNN-based prediction model performed multiple times under the same hyperparameter setting are different. Therefore, it conforms to the Bayesian optimization under the noisy environment. Fig. 12 increases the noise error bars compared to Fig. 1, and the error at the observation point is not 0.

Fig. 12 shows the effect of a single hyperparameter on the prediction model. Next, the effect of the two hyperparameters on the predictive model will be discussed. There are 5 hyperparameters discussed including network depth, learning rate, momentum, batch size, and L2 regularization. Two of the five hyperparameters were randomly selected as a group, and there were 10 groups. Fig. 13 shows the effect of 10 different groups of parameters on the prediction model. The red surface shown in Fig.13 is model mean representing the effect of two hyperparameters on the predictive model. The blue dots, black dots, and red star points have the same meaning as in Fig. 12. The z-coordinate of Fig. 13 represents the E_{RMSE} value of the FD001 sub-dataset test results, and RMSE is used in the figure instead.

The network depth in the 5 hyperparameters is a discrete integer containing only 1, 2, and 3. The other hyperparameters are consecutive numbers in the range. Therefore, the surface of Fig. 13(a), Fig. 13(b), Fig. 13(c), and Fig. 13(d) containing the network depth has a fracture phenomenon. And the surface of other graphs is continuous. The contoured lines on the bottom of the graphs correspond to changes of the red surface, whereas the blue color represents a smaller value and the yellow color represents a larger value.

Next, the results obtained by the Bayesian optimization is compared with the grid search and the random search. The results of finding the best hyperparameters using the Bayesian optimization method have been provided in Table 6. Tables 9 and 10 are the results of using grid search and random search methods, respectively. The tables contain 5 hyperparameters: learning rates (LR), network depth (Depth), momentum (Mo), batch size (Bs), and L2 regularization (L2). The number of iterations is denoted by #. The test E_{RMSE} of the FD001 test dataset is also shown in the table.

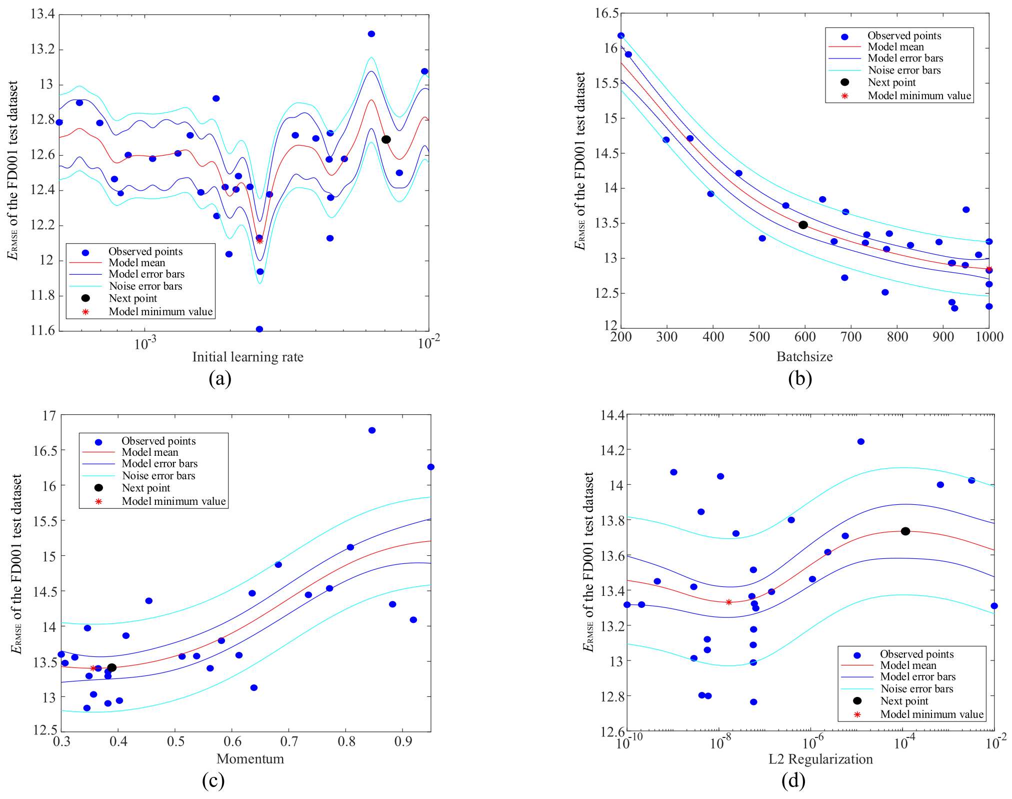

FIGURE 12. The influence of single hyperparameters on prediction model: (a) Initial learning rate, (b) Batchsize, (c) Momentum, and (d) L2 regularization.

TABLE 9. Grid search for multiple iterations to search for the best parameters in FD001.

#	E_{RMSE}	Depth	LR	Mo	Bs	L2	#	E_{RMSE}	Depth	LR	Mo	Bs	L2
1	13.40	1	1E-3	0.4	400	1E-3	25	12.78	2	5E-3	0.4	400	1E-3
2	13.26	1	1E-3	0.4	400	1E-6	26	13.97	2	5E-3	0.4	400	1E-6
3	13.35	1	1E-3	0.4	600	1E-3	27	13.47	2	5E-3	0.4	600	1E-3
4	13.43	1	1E-3	0.4	600	1E-6	28	13.59	2	5E-3	0.4	600	1E-6
5	13.65	1	1E-3	0.8	400	1E-3	29	13.60	2	5E-3	0.8	400	1E-3
6	14.47	1	1E-3	0.8	400	1E-6	30	13.15	2	5E-3	0.8	400	1E-6
7	13.98	1	1E-3	0.8	600	1E-3	31	13.17	2	5E-3	0.8	600	1E-3
8	14.46	1	1E-3	0.8	600	1E-6	32	14.19	2	5E-3	0.8	600	1E-6
9	14.24	1	5E-3	0.4	400	1E-3	**33**	**12.56**	**3**	**1E-3**	**0.4**	**400**	**1E-3**
10	13.03	1	5E-3	0.4	400	1E-6	34	13.76	3	1E-3	0.4	400	1E-6
11	12.64	1	5E-3	0.4	600	1E-3	35	14.25	3	1E-3	0.4	600	1E-3
12	12.88	1	5E-3	0.4	600	1E-6	36	12.77	3	1E-3	0.4	600	1E-6
13	13.08	1	5E-3	0.8	400	1E-3	37	14.48	3	1E-3	0.8	400	1E-3
14	14.00	1	5E-3	0.8	400	1E-6	38	12.77	3	1E-3	0.8	400	1E-6
15	14.31	1	5E-3	0.8	600	1E-3	39	13.42	3	1E-3	0.8	600	1E-3
16	14.25	1	5E-3	0.8	600	1E-6	40	12.62	3	1E-3	0.8	600	1E-6
17	13.64	2	1E-3	0.4	400	1E-3	41	13.22	3	5E-3	0.4	400	1E-3
18	13.67	2	1E-3	0.4	400	1E-6	42	13.45	3	5E-3	0.4	400	1E-6
19	12.84	2	1E-3	0.4	600	1E-3	43	13.02	3	5E-3	0.4	600	1E-3
20	12.86	2	1E-3	0.4	600	1E-6	44	13.29	3	5E-3	0.4	600	1E-6
21	13.47	2	1E-3	0.8	400	1E-3	45	13.13	3	5E-3	0.8	400	1E-3
22	13.26	2	1E-3	0.8	400	1E-6	46	12.62	3	5E-3	0.8	400	1E-6
23	13.81	2	1E-3	0.8	600	1E-3	47	14.11	3	5E-3	0.8	600	1E-3
24	13.43	2	1E-3	0.8	600	1E-6	48	14.05	3	5E-3	0.8	600	1E-6

The grid search method selected several values within the range of each hyperparameter and then selected a value for each hyperparameter to form a parameter combination. Finally, all the parameter combinations were used for training and testing and the parameter combination with the best prediction result was selected. In Table 9, the network depth has three values of 1, 2, and 3; the learning rate has two values 1E-3 and 5E-3; the momentum has two values 0.4 and 0.8; the batch size has two values 400 and 600; the L2 regularization has two values 1E-3 and 1E-6. Therefore, there are a total of 48 ($3 \times 2 \times 2 \times 2 \times 2 = 48$) parameter combinations. The 48 parameter combinations and their corresponding test

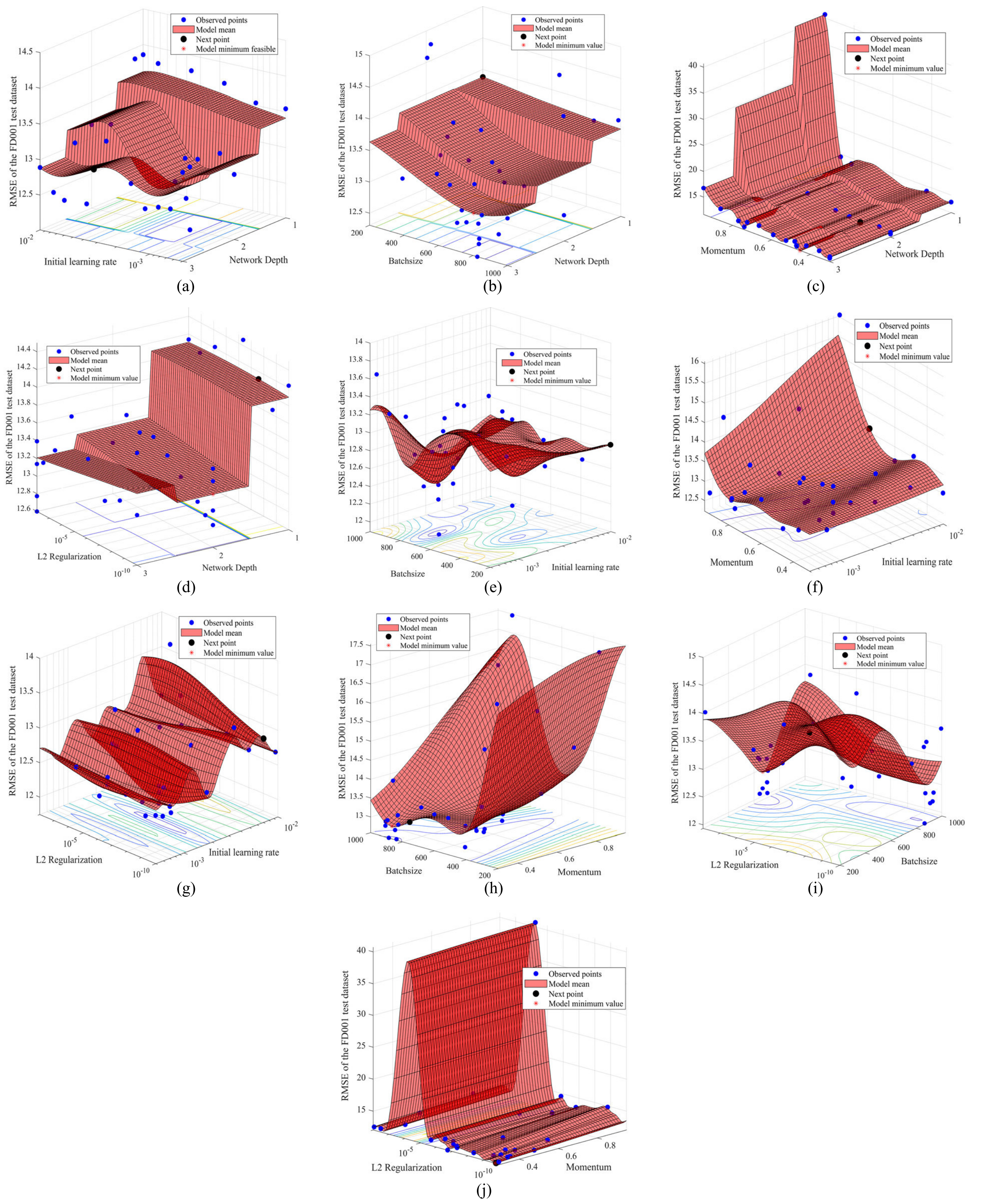

FIGURE 13. **The influence of two kinds of hyperparameters on prediction model: (a) Network depth-Initial learning rate, (b) Network depth-Batchsize, (c) Network depth-Momentum, (d) Network depth-L2 regularization, (e) Initial learning rate-Batchsize, (f) Initial learning rate- Momentum, (g) Initial learning rate-L2 regularization, (h) Batchsize-Momentum, (i) Batchsize-L2 regularization, and (j) Momentum-L2 regularization.**

E_{RMSE} values are shown in Table 9. The minimum prediction E_{RMSE} of 12.56 was obtained by #33 parameter combination. When the random search method was used, each hyperparameter value was randomly generated within the range for training. The random parameters training and results of 30 times are shown in Table 10. The network

TABLE 10. Random search for multiple iterations to search for the best parameters in FD001.

#	E_{RMSE}	Depth	LR	Mo	Bs	L2
1	12.92	1	6.74E-03	0.4133	677	2.00E-08
2	13.88	1	2.79E-03	0.9327	881	5.76E-10
3	12.65	1	1.85E-03	0.4739	215	8.23E-08
4	12.84	1	1.29E-03	0.8010	862	2.00E-07
5	13.81	1	8.22E-03	0.6778	870	2.08E-06
6	15.83	1	1.52E-03	0.6064	816	8.84E-10
7	12.61	1	5.51E-03	0.3626	905	1.90E-09
8	12.87	1	5.55E-04	0.5962	707	8.49E-05
9	12.51	1	6.03E-03	0.4526	483	8.85E-04
10	13.13	1	7.08E-04	0.4905	554	1.82E-03
11	13.37	2	6.10E-04	0.4585	619	8.86E-03
12	13.04	2	3.12E-03	0.8516	277	3.31E-03
13	14.39	2	4.50E-03	0.7835	335	3.82E-04
14	13.04	2	8.02E-03	0.5978	501	8.94E-03
15	12.53	2	2.28E-03	0.4621	588	2.83E-04
16	12.67	2	8.51E-04	0.5290	983	2.28E-06
17	14.67	2	2.04E-03	0.9455	731	3.71E-06
18	13.40	2	1.80E-03	0.4927	306	2.75E-07
19	13.08	2	3.46E-03	0.7225	609	9.67E-04
20	13.13	2	4.14E-03	0.8126	835	3.24E-10
21	13.14	3	1.67E-03	0.4287	376	2.11E-09
22	12.91	3	1.89E-03	0.4767	653	1.84E-05
23	14.88	3	6.73E-03	0.9477	451	5.46E-09
24	13.97	3	1.07E-03	0.8486	975	4.92E-05
25	12.46	3	6.46E-04	0.3918	767	1.09E-10
26	12.65	3	1.96E-03	0.6525	205	4.05E-07
27	14.39	3	7.05E-04	0.7066	897	1.12E-07
28	**12.32**	**3**	**8.66E-03**	**0.3879**	**502**	**1.60E-04**
29	12.41	3	1.57E-03	0.8877	448	1.63E-06
30	13.01	3	2.33E-03	0.6667	647	4.15E-07

TABLE 11. The best parameters selected by the Bayesian optimization with the TW length 18.

#	Running time /s	E_{RMSE}	Network Depth	Initial LR	Momentum	Batchsize	L2 Regularization
FD001	108.62	15.35	2	0.007139	0.30421	858	1.0557e-10
FD002	309.38	20.13	2	0.000650	0.91703	720	0.0084621
FD003	320.42	15.90	2	0.002096	0.32194	898	0.00055706
FD004	322.34	23.93	2	0.001778	0.45121	950	3.6048e-10

TABLE 12. The Cross Prediction results of the 4 sub-datasets.

	Source domain		FD001		FD002		FD003		FD004	
			E_{RMSE}	E_{sorce}	E_{RMSE}	E_{sorce}	E_{RMSE}	E_{sorce}	E_{RMSE}	E_{sorce}
Target domain	FD001	Without AdaBN	15.35	7.64×10^{2}	129.50	1.70×10^{19}	20.27	2.16×10^{3}	197.64	8.64×10^{25}
		AdaBN			17.31	6.78×10^{2}	17.69	8.14×10^{2}	18.20	9.46×10^{2}
	FD002	Without AdaBN	56.07	1.33×10^{6}	20.13	2.51×10^{3}	59.90	1.88×10^{6}	25.34	7.80×10^{3}
		AdaBN	26.08	6.76×10^{3}			27.14	1.08×10^{4}	24.85	6.76×10^{3}
	FD003	Without AdaBN	20.19	1.26×10^{3}	177.97	1.02×10^{18}	15.90	1.40×10^{3}	209.69	1.03×10^{21}
		AdaBN	17.87	1.05×10^{3}	18.23	1.54×10^{3}			18.08	1.49×10^{3}
	FD004	Without AdaBN	52.28	6.59×10^{5}	34.46	1.71×10^{4}	53.31	9.47×10^{5}	23.93	3.87×10^{3}
		AdaBN	32.26	2.86×10^{4}	29.95	9.53×10^{3}	31.05	1.56×10^{4}		

depth is an integer and contains only 3 values. Therefore, the grid search was adopted when selecting the network depth. And 10 trials were performed in each network depth. The minimum prediction E_{RMSE} of 12.32 was obtained by #28 parameter combination in the random search. Comparing the three parameter selection methods in Table 6, Table 9, and Table 10, the Bayesian optimization method is the best, and the random search method is slightly better than the grid search method.

There are m hyperparameters, and each hyperparameter selects n values, then there are a total of n^m kinds of parameter combinations for the grid search. The disadvantage of the grid search method is that all the parameter combinations are tried, and each attempt takes a lot of time and effort. Therefore, in order to avoid excessive computational times, it is necessary to reduce the number of values of each hyperparameter. However, too few values for each hyperparameter will affect the optimization results. The experimental results show that the random search method is better than grid search. However, there is no correlation between any two trials in the random search, so the stability of the search is poor. Compared to the above two parameter-finding method, Bayesian optimization can determine the next trial parameters based on the existing results. This allows for better predictions with fewer trials.

3) PREDICTION RESULTS IN DIFFERENT DATA DOMAINS

The application of data-driven prediction methods does not require a deep understanding of the mechanical equipment, relying solely on data to develop a prediction model. However, when the test data differs greatly from the data used for the training model, the accuracy of the prediction is low. Retraining the model is time consuming and laborious, so the ability of the model to adapt to different DDs is very important. In this paper, the BN unit is added to the model. When the test DD changes, adjusting the offset and scale factor in the BN unit can quickly adapt the model to the new DD. The 4 sub-datasets in CMAPSS were used to test the ability of the proposed prediction model to adapt to different DDs. In order to make the input data size of the 4 sub-datasets consistent, the window length during data processing was all set to 18. Table 11 shows the results of hyperparameter

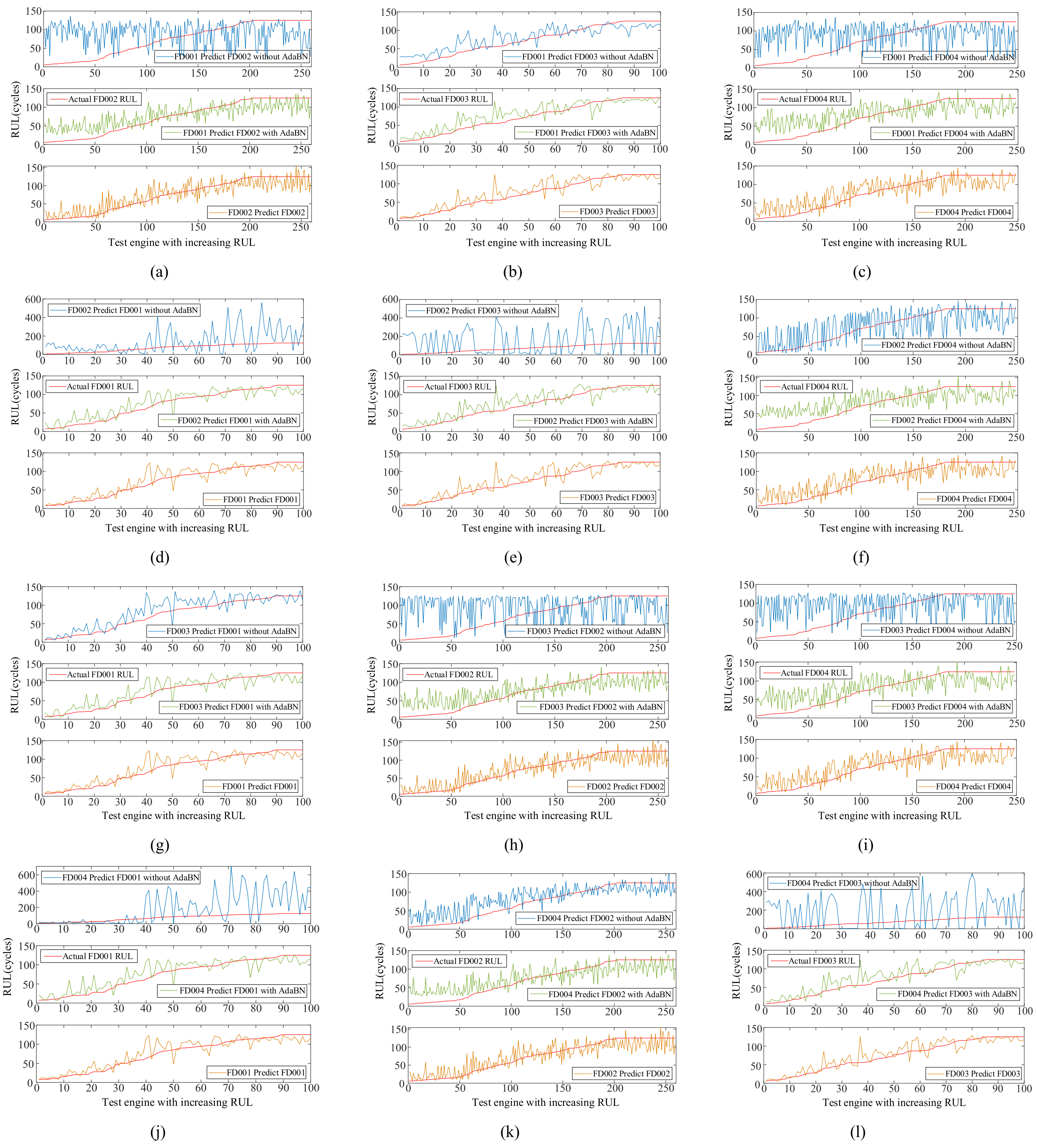

FIGURE 14. **Comparison of the improvement of AdaBN in cross prediction: (a) FD001→FD002, (b) FD001→FD003, (c) FD001→FD004, (d) FD002→FD001, (e) FD002→FD003, (f) FD002→FD004, (g) FD003→FD001, (h) FD003→FD002, (i) FD003→FD004, (j) FD004→FD001, (k) FD004→FD002, and (l) FD004→FD003.**

selection for Bayesian optimization of 4 sub-datasets with the WT length of 18. This section is intended to discuss the ability of the prediction model to predict different DDs. The sliding steps of the 4 sub-datasets convolution filters were all set to [2, 1]. Hence, the running time of the 4 datasets was similar. Since the input data time series length was shortened to 18, the diagnostic E_{RMSE} in Table 11 is slightly larger than that in Table 7. And the 5 hyperparameters were selected in the same way as above.

Table 12 shows the results of cross prediction of 4 sub-datasets. The source domain was the data used to train the prediction model, and the target domain was the data domain used in the test. The prediction results include both E_{RMSE} and E_{sorce}. It also compares the results of the fine-tuning the network with or without the AdaBN method. It can be seen from the Table 12 that the prediction results can be improved after the fine-tuning by the proposed AdaBN method. In particular, the E_{RMSE} fine-tuned by the AdaBN method in the 4 cases of FD002→FD001, FD002→FD003, FD004→FD001, and FD004→FD003 is reduced by nearly 10 times. In addition, the E_{RMSE} fine-tuned by the AdaBN method in the 4 cases of FD001→FD002, FD001→FD004, FD003→FD002, and FD003→FD004 is reduced by nearly 2 times. In other cases, the improvement effect of AdaBN is also obvious.

Fig. 14 compare the results of the cross DD prediction with or without the AdaBN fine-tuned network. The three graphs in Fig. 14(a-c) are based on FD001 as the source domain training model, and the other 3 sub-datasets are used as target domains for testing. The prediction results in the three cases in Fig. 14(a) are: (1) prediction of the RUL of the FD002 using the model trained by FD001 without AdaBN; (2) prediction of the RUL of the FD002 using the model trained by FD001 with AdaBN; (3) prediction of the RUL of the FD002 using the model trained by FD002. It can be seen intuitively from Fig. 14 that the prediction results after AdaBN fine-tuning have been significantly improved. And it is close to the prediction results that are trained and tested with the same DD. Fig. 14(a-c) correspond to the FD001 column in Table 11. The following Fig. 14(d-f), Fig. 14(g-i), and Fig. 14(j-l) are cross-predictions with FD002, FD003, and FD004 as the source domains, respectively. Table 4 shows that FD001 and FD003 contain fewer fault modes and operating conditions, and more fault modes and operating conditions are included in FD002 and FD004. Combined with Table 12 and Fig. 14, it can be concluded that AdaBN performs better when predicting the DD with fewer fault modes and operating conditions using models trained in a DD with more fault modes and operating conditions.

V. CONCLUSION

This paper presented a novel RUL prediction model developed using a DCNN combined with Bayesian optimization and AdaBN. The model has a self-optimized structure and hyperparameters of DCNN. The Bayesian optimization was integrated into DCNN to achieve automatic structure and hyperparameter selection. In addition, in order to improve the ability of the prediction model to adapt to multiple DDs, BN units and AdaBN fine-tuning strategy were also integrated. The proposed prediction method was validated by the CMAPSS simulated turbofan engine dataset. The prediction performance of the proposed method was compared with other prediction methods validated by the CMAPSS dataset in the past 4 years. The comparison results show that the performance of the proposed prediction method is better than other methods. The following conclusions can also be obtained:

(1) The 4 sub-datasets in CMAPSS were all used to test the proposed self-optimization prediction method. The prediction results of the FD001 and FD003 sub-datasets with fewer operating conditions and fault modes are better. Both E_{RMSE} and E_{sorce} show that the overall prediction results of the proposed method are better than other prediction methods in the past 4 years.

(2) The Bayesian optimization method finds the best combination of hyperparameters through multiple iterations. Comparing the grid search and the random search, the Bayesian method can obtain better prediction results with fewer iterations. And the Bayesian optimization method can intuitively reflect the relationship between the hyperparameters and the prediction results through the fitted curve or surface.

(3) Adding BN units to the model and fine-tuning the network through the AdaBN method when predicting different DDs can make the prediction model work better. The proposed AdaBN fine-tuning strategy can avoids the loss of time and effort in retraining the model. And the results obtained are close to the prediction results of training and testing using the same DD. In addition, it can be concluded that AdaBN performs better when predicting simple DD using models trained in complex DD.

REFERENCES

[1] K. L. Tsui, N. Chen, Q. Zhou, Y. Hai, and W. Wang, "Prognostics and health management: A review on data driven approaches," *Math. Problems Eng.*, vol. 2015, pp. 1–17, May 2015, doi: 10.1155/2015/793161.

[2] Y. Cao, W. Wei, C. Wang, S. Mei, S. Huang, and X. Zhang, "Probabilistic estimation of wind power ramp events: A data-driven optimization approach," *IEEE Access*, vol. 7, pp. 23261–23269, 2019.

[3] L. Liu, Q. Guo, D. Liu, and Y. Peng, "Data-driven remaining useful life prediction considering sensor anomaly detection and data recovery," *IEEE Access*, vol. 7, pp. 58336–58345, 2019.

[4] D. N. T. How, M. A. Hannan, M. S. H. Lipu, and P. J. Ker, "State of charge estimation for lithium-ion batteries using model-based and data-driven methods: A review," *IEEE Access*, vol. 7, pp. 136116–136136, 2019.

[5] R. Zhao, R. Yan, Z. Chen, K. Mao, P. Wang, and R. X. Gao, "Deep learning and its applications to machine health monitoring," *Mech. Syst. Signal Process.*, vol. 115, pp. 213–237, Jan. 2019, doi: 10.1016/j.ymssp.2018.05.050.

[6] L. Ren, Y. Sun, H. Wang, and L. Zhang, "Prediction of bearing remaining useful life with deep convolution neural network," *IEEE Access*, vol. 6, pp. 13041–13049, 2018.

[7] W. Yu, I. Y. Kim, and C. Mechefske, "Remaining useful life estimation using a bidirectional recurrent neural network based autoencoder scheme," *Mech. Syst. Signal Process.*, vol. 129, pp. 764–780, Aug. 2019, doi: 10.1016/j.ymssp.2019.05.005.

[8] S. Zhao, Y. Zhang, S. Wang, B. Zhou, and C. Cheng, "A recurrent neural network approach for remaining useful life prediction utilizing a novel trend features construction method," *Measurement*, vol. 146, pp. 279–288, Nov. 2019, doi: 10.1016/j.measurement.2019.06.004.

[9] A. Elsheikh, S. Yacout, and M.-S. Ouali, "Bidirectional handshaking LSTM for remaining useful life prediction," *Neurocomputing*, vol. 323, pp. 148–156, Jan. 2019, doi: 10.1016/j.neucom.2018.09.076.

[10] Y. Wu, M. Yuan, S. Dong, L. Lin, and Y. Liu, "Remaining useful life estimation of engineered systems using vanilla LSTM neural networks," *Neurocomputing*, vol. 275, pp. 167–179, Jan. 2018, doi: 10.1016/j.neucom.2017.05.063.

[11] M. Rigamonti, P. Baraldi, E. Zio, I. Roychoudhury, K. Goebel, and S. Poll, "Ensemble of optimized echo state networks for remaining useful life prediction," *Neurocomputing*, vol. 281, pp. 121–138, Mar. 2018, doi: 10.1016/j.neucom.2017.11.062.

[12] L. Yang, F. Wang, J. Zhang, and W. Ren, "Remaining useful life prediction of ultrasonic motor based on elman neural network with improved particle swarm optimization," *Measurement*, vol. 143, pp. 27–38, Sep. 2019, doi: 10.1016/j.measurement.2019.05.013.

[13] X. Li, W. Zhang, and Q. Ding, "Deep learning-based remaining useful life estimation of bearings using multi-scale feature extraction," *Rel. Eng. Syst. Saf.*, vol. 182, pp. 208–218, Feb. 2019, doi: 10.1016/j.ress.2018.11.011.

[14] J. Zhu, N. Chen, and W. Peng, "Estimation of bearing remaining useful life based on multiscale convolutional neural network," *IEEE Trans. Ind. Electron.*, vol. 66, no. 4, pp. 3208–3216, Apr. 2019, doi: 10.1109/TIE.2018.2844856.

[15] J. S. Bergstra, R. Bardenet, Y. Bengio, and B. Kégl, "Algorithms for hyper-parameter optimization," in *Proc. Neural Inf. Process. Syst. Conf.*, Granada, Spain, 2011, pp. 2546–2554.

[16] D. Sen, A. Aghazadeh, A. Mousavi, S. Nagarajaiah, R. Baraniuk, and A. Dabak, "Data-driven semi-supervised and supervised learning algorithms for health monitoring of pipes," *Mech. Syst. Signal Process.*, vol. 131, pp. 524–537, Sep. 2019, doi: 10.1016/j.ymssp.2019.06.003.

[17] Z. Tian, L. Wong, and N. Safaei, "A neural network approach for remaining useful life prediction utilizing both failure and suspension histories," *Mech. Syst. Signal Process.*, vol. 24, no. 5, pp. 1542–1555, Jul. 2010, doi: 10.1016/j.ymssp.2009.11.005.

[18] J. Bergstra and Y. Bengio, "Random search for hyper-parameter optimization," *J. Mach. Learn. Res.*, vol. 12, pp. 281–305, Feb. 2012.

[19] S. J. Pan and Q. Yang, "A survey on transfer learning," *IEEE Trans. Knowl. Data Eng.*, vol. 22, no. 10, pp. 1345–1359, Oct. 2010, doi: 10.1109/TKDE.2009.191.

[20] B. Yang, Y. Lei, F. Jia, and S. Xing, "An intelligent fault diagnosis approach based on transfer learning from laboratory bearings to locomotive bearings," *Mech. Syst. Signal Process.*, vol. 122, pp. 692–706, May 2019, doi: 10.1016/j.ymssp.2018.12.051.

[21] A. Zhang, H. Wang, S. Li, Y. Cui, Z. Liu, G. Yang, and J. Hu, "Transfer learning with deep recurrent neural networks for remaining useful life estimation," *Appl. Sci.*, vol. 8, no. 12, p. 2416, Nov. 2018, doi: 10.3390/app8122416.

[22] J. Wang, S. Li, Z. An, X. Jiang, W. Qian, and S. Ji, "Batch-normalized deep neural networks for achieving fast intelligent fault diagnosis of machines," *Neurocomputing*, vol. 329, pp. 53–65, Feb. 2019, doi: 10.1016/j.neucom.2018.10.049.

[23] D. Xiao, Y. Huang, C. Qin, H. Shi, and Y. Li, "Fault diagnosis of induction motors using recurrence quantification analysis and LSTM with weighted BN," *Shock Vib.*, vol. 2019, pp. 1–14, Jan. 2019, doi: 10.1155/2019/8325218.

[24] L. Bottou, "Stochastic gradient descent tricks," in *Neural Networks: Tricks Trade*, vol. 7700, G. Montavon, G. B. Orr, and K.-R. Müller, Eds. Berlin, Germany: Springer, 2012, pp. 421–436, doi: 10.1007/978-3-642-35289-8_25.

[25] B. Shahriari, K. Swersky, Z. Wang, R. P. Adams, and N. de Freitas, "Taking the human out of the loop: A review of Bayesian optimization," *Proc. IEEE*, vol. 104, no. 1, pp. 148–175, Jan. 2016, doi: 10.1109/JPROC.2015.2494218.

[26] C. E. Rasmussen and C. K. I. Williams, *Gaussian Processes for Machine Learning*. Cambridge, MA, USA: Massachusetts Institute of Technology, 2006. [Online]. Available: https://www.GaussianProcess.org/gpml

[27] C. E. Rasmussen, "Gaussian processes in machine learning," in *Advanced Lectures on Machine Learning*, vol. 3176, O. Bousquet, U. von Luxburg, and G. Rätsch, Eds. Berlin, Germany: Springer, 2004, pp. 63–71, doi: 10.1007/978-3-540-28650-9_4.

[28] J. Snoek, H. Larochelle, and R. P. Adams, "Practical Bayesian optimization of machine learning algorithms," in *Advances in Neural Information Processing Systems*, 2012, pp. 2951–2959.

[29] E. Brochu, V. M. Cora, and N. de Freitas, "A tutorial on Bayesian optimization of expensive cost functions, with application to active user modeling and hierarchical reinforcement learning," 2010, *arXiv:1012.2599*. [Online]. Available: http://arxiv.org/abs/1012.2599

[30] W. Wang, J. Shen, and L. Shao, "Video salient object detection via fully convolutional networks," *IEEE Trans. Image Process.*, vol. 27, no. 1, pp. 38–49, Jan. 2018, doi: 10.1109/TIP.2017.2754941.

[31] K. Fukushima, "Neocognitron: A self-organizing neural network model for a mechanism of pattern recognition unaffected by shift in position," *Biol. Cybern.*, vol. 36, no. 4, pp. 193–202, Apr. 1980, doi: 10.1007/BF00344251.

[32] G. E. Hinton, S. Osindero, and Y.-W. Teh, "A fast learning algorithm for deep belief nets," *Neural Comput.*, vol. 18, no. 7, pp. 1527–1554, Jul. 2006, doi: 10.1162/neco.2006.18.7.1527.

[33] X. Li, Q. Ding, and J.-Q. Sun, "Remaining useful life estimation in prognostics using deep convolution neural networks," *Rel. Eng. Syst. Saf.*, vol. 172, pp. 1–11, Apr. 2018, doi: 10.1016/j.ress.2017.11.021.

[34] N. Srivastava, G. Hinton, A. Krizhevsky, I. Sutskever, and R. Salakhutdinov, "Dropout: A simple way to prevent neural networks from overfitting," *J. Mach. Learn. Res.*, vol. 15, pp. 1929–1958, 2014.

[35] D. Hutchison, "Evaluation of pooling operations in convolutional architectures for object recognition," in *Artificial Neural Networks*, vol. 6354, K. Diamantaras, W. Duch, and L. S. Iliadis, Eds. Berlin, Germany: Springer, 2010, pp. 92–101, doi: 10.1007/978-3-642-15825-4_10.

[36] Y. Li, N. Wang, J. Shi, X. Hou, and J. Liu, "Adaptive batch normalization for practical domain adaptation," *Pattern Recognit.*, vol. 80, pp. 109–117, Aug. 2018, doi: 10.1016/j.patcog.2018.03.005.

[37] A. Saxena, K. Goebel, D. Simon, and N. Eklund, "Damage propagation modeling for aircraft engine run-to-failure simulation," in *Proc. Int. Conf. Prognostics Health Manage.*, Denver, CO, USA, Oct. 2008, pp. 1–9, doi: 10.1109/PHM.2008.4711414.

[38] J. Wang, G. Wen, S. Yang, and Y. Liu, "Remaining useful life estimation in prognostics using deep bidirectional LSTM neural network," in *Proc. Prognostics Syst. Health Manage. Conf. (PHM-Chongqing)*, Chongqing, China, 2018, pp. 1037–1042, doi: 10.1109/PHM-Chongqing.2018.00184.

[39] G. S. Babu, P. Zhao, and X.-L. Li, "Deep convolutional neural network based regression approach for estimation of remaining useful life," in *Database Systems for Advanced Applications*, vol. 9642, S. B. Navathe, W. Wu, S. Shekhar, X. Du, X. S. Wang, and H. Xiong, Eds. Cham, Switzerland: Springer, 2016, pp. 214–228, doi: 10.1007/978-3-319-32025-0_14.

[40] S. Zheng, K. Ristovski, A. Farahat, and C. Gupta, "Long short-term memory network for remaining useful life estimation," in *Proc. IEEE Int. Conf. Prognostics Health Manage. (ICPHM)*, Dallas, TX, USA, Jun. 2017, pp. 88–95, doi: 10.1109/ICPHM.2017.7998311.

[41] C. Zhang, P. Lim, A. K. Qin, and K. C. Tan, "Multiobjective deep belief networks ensemble for remaining useful life estimation in prognostics," *IEEE Trans. Neural Netw. Learn. Syst.*, vol. 28, no. 10, pp. 2306–2318, Oct. 2017, doi: 10.1109/TNNLS.2016.2582798.

[42] J. Li, X. Li, and D. He, "A directed acyclic graph network combined with CNN and LSTM for remaining useful life prediction," *IEEE Access*, vol. 7, pp. 75464–75475, 2019, doi: 10.1109/ACCESS.2019.2919566.

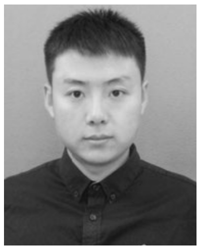

JIALIN LI was born in Shenyang, China. He received the B.E. degree from the School of Mechanical Engineering, Shenyang University of Technology, China, and the M.S. degree from the School of Mechanical Engineering and Automation, Northeastern University, China, where he is currently pursuing the Ph.D. degree with the School of Mechanical Engineering and Automation. His current research interests include data-driven methods to fault diagnosis, pattern recognition, deep learning, and remaining useful life estimation and their applications to critical components of mechanical equipment.

DAVID HE received the B.S. degree in metallurgical engineering from the Shanghai University of Technology, China, the M.B.A. degree from the University of Northern Iowa, and the Ph.D. degree in industrial engineering from the University of Iowa, in 1994. He is currently a Professor and the Director of the Intelligent Systems Modeling and Development Laboratory, Department of Mechanical and Industrial Engineering, The University of Illinois at Chicago, Chicago. His research areas include machinery health monitoring, diagnosis and prognosis, complex systems failure analysis, quality and reliability engineering, and manufacturing systems design, modeling, scheduling, and planning.